HHS Public Access

Author manuscript

Nature. Author manuscript; available in PMC 2021 October 07.

Published in final edited form as:

Nature. 2020 October ; 586(7829): 412–416. doi:10.1038/s41586-020-2805-8.

eIF2α controls memory consolidation via excitatory and somatostatin neurons

Vijendra Sharma[1,2,†], **Rapita Sood**[1,2,19], **Abdessattar Khlaifia**[3,19], **Mohammad Javad Eslamizade**[1,2,3,19], **Tzu-Yu Hung**[1,2], **Danning Lou**[1,2], **Azam Asgarihafshejani**[3], **Maya Lalzar**[4], **Stephen J. Kiniry**[5], **Matthew P. Stokes**[6], **Noah Cohen**[1,2], **Alissa J. Nelson**[6], **Kathryn Abell**[6], **Anthony P. Possemato**[6], **Shunit Gal-Ben-Ari**[7], **Vinh T. Truong**[1,2], **Peng Wang**[1,2], **Adonis Yiannakas**[7], **Fatemeh Saffarzadeh**[3], **A. Claudio Cuello**[8], **Karim Nader**[9], **Randal J. Kaufman**[10], **Mauro Costa-Mattioli**[11], **Pavel V. Baranov**[5,12], **Albert Quintana**[13,14], **Elisenda Sanz**[13,14], **Arkady Khoutorsky**[15,16,20], **Jean-Claude Lacaille**[3,17,20], **Kobi Rosenblum**[7,18,20,†], **Nahum Sonenberg**[1,2,20,†]

[1]Department of Biochemistry, McGill University, Montréal, Québec, Canada. [2]Rosalind and Morris Goodman Cancer Research Centre, McGill University, Montréal, Québec, Canada. [3]Department of Neurosciences, University of Montréal, Montréal, Québec, Canada. [4]Bioinformatics Services Unit, Faculty of Natural Sciences, University of Haifa, Mount Carmel, Haifa, Israel. [5]School of Biochemistry and Cell Biology, University College Cork, Cork T12 XF62, Ireland. [6]Proteomics Division, Cell Signaling Technology, Danvers, MA, 01923., USA. [7]Sagol Department of Neurobiology, University of Haifa, Haifa, Israel. [8]Department of Pharmacology and Therapeutics, McGill University, Montréal, Québec, Canada. [9]Department of Psychology, McGill University, Montréal, Québec, Canada. [10]Degenerative Diseases Program, Sanford-Burnham-Prebys Medical Discovery Institute, La Jolla, CA, USA. [11]Department of Neuroscience, Baylor College of Medicine, Houston, TX, USA. [12]Shemyakin and Ovchinnikov Institute of Bioorganic Chemistry, RAS, Moscow, Russia. [13]Department of Cell Biology, Physiology and Immunology, Universitat Autònoma de Barcelona, Bellaterra, Spain. [14]Neuroscience Institute, Universitat Autònoma de Barcelona, Bellaterra, Spain. [15]Department of Anesthesia, McGill University, Montréal, Québec, Canada. [16]Faculty of Dentistry, McGill University, Montréal, Québec, Canada. [17]Centre for Interdisciplinary Research on Brain and Learning, University of Montréal, Montréal, Québec,

[†]Corresponding authors Correspondence to Vijendra Sharma or Kobi Rosenblum or Nahum Sonenberg. vijendra.sharma@mcgill.ca, kobir@psy.haifa.ac.il, nahum.sonenberg@mcgill.ca.

Contributions

V.S., A. Khoutorsky, J.-C.L., K.R. and N.S. conceived the project, designed experiments and supervised the research. V.S., R.S., T.-Y.H., D.L. and N.C. designed and set up mouse breeding. V.S., R.S., T.-Y.H., D.L., N.C. and V.T.T. performed the stereotaxic surgery, cannula implantation and microinjection. V.S., R.S., T.-Y.H. and D.L. carried out iSUnSET and FUNCAT. A. Khlaifia, A.A. and M.J.E. carried out whole-cell recording and analysis. V.S., A. Khlaifia, A.A., M.J.E. and F.S. carried out field potential recordings and analysis. V.S., R.S., T.-Y.H., D.L. and N.C. carried out behaviour tests, immunohistochemistry and image analysis. V.S., R.S., T.-Y.H., D.L., M.L., M.P.S., A.J.N., K.A. and A.P.P. carried out sample preparation and LC–MS/MS analysis. V.S., E.S., M.L., S.J.K., R.S., T.-Y.H., D.L. and P.W. carried out RiboTag assays, RNA sequencing library preparation and analysis. V.S., R.S., A. Khlaifia, T.-Y.H., D.L., A.A., M.L., N.C., S.J.K., E.S., P.V.B., M.C.-M., A. Khoutorsky, J.-C.L., K.R. and N.S. wrote the manuscript. S.G.-B.-A., A.C.C., K.N., A.Q. and R.J.K. supported the experiments. All authors reviewed the manuscript and discussed the work.

Ethics declarations

Competing interests

The authors declare no competing interests.

Additional information

Peer review information *Nature* thanks the anonymous reviewers for their contribution to the peer review of this work.

Canada [18]Center for Gene Manipulation in the Brain, University of Haifa, Haifa, Israel. [19]These authors contributed equally: Rapita Sood, Abdessattar Khlaifia, Mohammad Javad Eslamizade. [20]These authors jointly supervised this work: Arkady Khoutorsky, Jean-Claude Lacaille, Kobi Rosenblum, Nahum Sonenberg.

Abstract

An important tenet of learning and memory is the notion of a molecular switch that promotes the formation of long-term memory[1,2,3,4]. The regulation of proteostasis is a critical and rate-limiting step in the consolidation of new memories[5,6,7,8,9,10]. One of the most effective and prevalent ways to enhance memory is by regulating the synthesis of proteins controlled by the translation initiation factor eIF2[11]. Phosphorylation of the α-subunit of eIF2 (p-eIF2α), the central component of the integrated stress response (ISR), impairs long-term memory formation in rodents and birds[11,12,13]. By contrast, inhibiting the ISR by mutating the eIF2α phosphorylation site, genetically[11] and pharmacologically inhibiting the ISR kinases[14,15,16,17], or mimicking reduced p-eIF2α with the ISR inhibitor ISRIB[11], enhances long-term memory in health and disease[18]. Here we used molecular genetics to dissect the neuronal circuits by which the ISR gates cognitive processing. We found that learning reduces eIF2α phosphorylation in hippocampal excitatory neurons and a subset of hippocampal inhibitory neurons (those that express somatostatin, but not parvalbumin). Moreover, ablation of p-eIF2α in either excitatory or somatostatin-expressing (but not parvalbumin-expressing) inhibitory neurons increased general mRNA translation, bolstered synaptic plasticity and enhanced long-term memory. Thus, eIF2α-dependent mRNA translation controls memory consolidation via autonomous mechanisms in excitatory and somatostatin-expressing inhibitory neurons.

To identify which neuronal subtypes mediate the effect of reduced p-eIF2α on memory formation, we first studied in which neurons the amount of p-eIF2α is decreased after learning. Mice were subjected to fear conditioning and their brains were fixed and immunostained for p-eIF2α and markers of excitatory neurons and the two largest defined subclasses of inhibitory neurons (parvalbumin (PVALB)- and somatostatin (SST)-expressing), in the CA1 region of the dorsal hippocampus. Fear conditioning caused a substantial reduction in p-eIF2α in excitatory (20.83 ± 5.9% (mean ± s.e.m.)) and SST^+ neurons (17.64 ± 4.46%), but not in $PVALB^+$ neurons (Extended Data Fig. 1a–h). Metabolic labelling showed that learning induced an increase in protein synthesis in excitatory neurons (21.67 ± 3.91%) and SST^+ inhibitory neurons (14.33 ± 3.64%) but not in $PVALB^+$ inhibitory neurons, consistent with extensive evidence that a decrease in p-eIF2α causes an increase in protein synthesis (Extended Data Fig. 1i–m).

Cell-type-specific ablation of p-eIF2α

To study the consequences of reducing p-eIF2α in different neuronal subtypes during learning and memory, we generated transgenic mice in which phosphorylation of eIF2α was ablated in excitatory or inhibitory neurons. We used a transgenic mouse harbouring both the non-phosphorylatable Ser51Ala mutant *Eif2a* gene ($Eif2a^{A/A}$) and the wild-type *Eif2a* transgene driven by the CMV enhancer and chicken β-actin promoter (Enh-Pro)[19]. The

wild-type *Eif2a* transgene is flanked by *LoxP* sites (floxed transgene, *fTg*) and is excised upon expression of Cre recombinase, which also induces the expression of enhanced GFP (eGFP). Ablation of p-eIF2α in excitatory neurons in the forebrain was achieved by crossing *Eif2a*$^{A/A}$*fTg*$^{+}$ mice with mice expressing Cre recombinase under the promoter of the Ca^{2+}-calmodulin-dependent protein kinase IIα (*Camk2a*) (Fig. 1a, b). Immunostaining of the CA1 region of *Eif2a*$^{A/A}$*fTg*$^{+}$*Camk2a*-Cre^{+} conditional knock-in mice (*Eif2a* cKI^{Camk2a}) confirmed the selective elimination of p-eIF2α in excitatory neurons (Fig. 1c, Extended Data Fig. 2a, b). The reduction of p-eIF2α promotes the formation of ternary complexes and initiation of translation[20]. We, therefore, used the puromycin incorporation assay to assess protein synthesis in brain sections from *Eif2a*$^{A/A}$*fTg*$^{+}$ mice injected with adeno-associated virus expressing Cre recombinase under the *Camk2a* promotor (AAV9-*Camk2a*-Cre). As expected, an increase of 20.32 ± 2.26% in puromycin incorporation was detected in excitatory neurons in the hippocampal CA1 region (Extended Data Fig. 2e–g), showing that enhancement of protein synthesis is a consequence of reduction in p-eIF2α.

p-eIF2α ablation in excitatory neurons

To study the effect of p-eIF2α on memory consolidation in excitatory neurons, we subjected *Eif2a* cKI^{Camk2a} mice to a fear conditioning test using a weak training protocol in which a tone was paired with a mild foot shock[11] (Fig. 1d). No differences in short-term memory (STM) were found between *Eif2a* cKI^{Camk2a} and control mice (*Eif2a*$^{A/A}$*fTg*$^{+}$ and *Camk2a*-Cre^{+}), as all groups exhibited similar freezing 1 h after contextual and cued fear conditioning (Extended Data Fig. 2c, d). However, 24 h after training, *Eif2a* cKI^{Camk2a} mice froze substantially more than control mice (*Eif2a* cKI^{Camk2a}, 55 ± 5.3%; *Eif2a*$^{A/A}$*fTg*$^{+}$, 33.1 ± 3.4%; *Camk2a*-Cre^{+}, 34.1 ± 2.6%) in the conditioned context (context A; Fig. 1e). A similar result was obtained in an auditory fear conditioning task, performed in context B, which differed from context A to minimize the influence of contextual memory (Fig. 1f). *Eif2a* cKI^{Camk2a} mice also exhibited more freezing 24 h after strong training in both contextual (increase of 43.26 ± 6.9%) and cued (increase of 38.82 ± 8.08%) fear memory tasks (Extended Data Fig. 2h–j). No differences were found between *Eif2a* cKI^{Camk2a} mice and control mice in the open field test (Extended Data Fig. 2k–m), ruling out an anxiety-dependent phenotype. These results show that selective reduction of p-eIF2α in excitatory neurons of the forebrain enhances memory consolidation.

To corroborate these findings, we injected AAV9-*Camk2a*-Cre or AAV9-*Camk2a*-eGFP (control) bilaterally into the CA1 region of the dorsal hippocampus of *Eif2a*$^{A/A}$*fTg*$^{+}$ adult mice (Extended Data Fig. 3a, b). Mice injected with AAV9-*Camk2a*-Cre showed enhanced contextual fear memory 1 and 15 days after training (Extended Data Fig. 3c, d; increase of 59.91 ± 20.11% after day 1 and increase of 38.01 ± 12.02% after 15 days) with no effect on hippocampus-independent auditory fear memory or anxiety-like behaviour (Extended Data Fig. 3e, f). Moreover, bilateral injection of AAV9-*Camk2a*-Cre into the amygdala substantially enhanced both contextual (increase of 37.03 ± 7.64% after day 1 and 42.7 ± 11.04% after 15 days) and auditory fear responses (Extended Data Fig. 3g–j; increase of 36.55 ± 8.47% after day 1) without affecting behaviour in an open field test (Extended Data Fig. 3k). Hence, selective reduction of p-eIF2α in excitatory neurons is sufficient to enhance long-term memory (LTM).

Long-term potentiation (LTP) is the putative mechanism for learning processes[21,22]. The early phase of long-term potentiation (E-LTP) is not dependent on protein synthesis[23], whereas de novo protein synthesis is required for late-phase LTP (L-LTP). A general decrease in phosphorylation of eIF2α results in a lower threshold for eliciting L-LTP[11,17]. Thus, we assessed LTP by measuring field excitatory postsynaptic potentials (fEPSPs) in the CA1 stratum radiatum of acute hippocampal slices from *Eif2a*$^{A/A}$*fTg*$^{+}$ mice injected with AAV9-*Camk2a*-Cre or AAV9-*Camk2a*-eGFP (control). In mice injected with AAV9-*Camk2a*-eGFP, a single train of high-frequency stimulation (1 × HFS) of Schaffer collaterals elicited short-lasting E-LTP of fEPSPs (Fig. 1g, h, Extended Data Fig. 3l, m). By contrast, in mice injected with AAV9-*Camk2a*-Cre, the same stimulation protocol (1 × HFS) induced long-lasting L-LTP. More intense stimulation consisting of four trains of HFS (4 × HFS) elicited similar L-LTP in *Eif2a*$^{A/A}$*fTg*$^{+}$ mice injected with AAV9-*Camk2a*-Cre or AAV9-*Camk2a*-eGFP (Extended Data Fig. 3n, o). We found no alteration in paired-pulse facilitation (PPF) in slices in which p-eIF2α was ablated in excitatory neurons (Extended Data Fig. 3p). Whole cell patch-clamp recording showed that reducing p-eIF2α in CA1 excitatory neurons increased the amplitude and frequency of miniature excitatory postsynaptic currents (mEPSCs; Fig. 1i–l) and decreased the frequency of miniature inhibitory postsynaptic currents (mIPSCs; Fig. 1m–p). It also caused a slight depolarization of the resting membrane potential (7.21 ± 2.16 mV) without changing cell input resistance (*R*in) or the frequency of evoked action potential firing (Extended Data Fig. 3q–u). Thus, reducing p-eIF2α promotes an increase in excitatory and a decrease in inhibitory synaptic inputs onto pyramidal neurons, lowers the threshold for induction of persistent synaptic potentiation, and facilitates the conversion of early LTP into late LTP.

Changes in protein synthesis in excitatory neurons

To study the effect of p-eIF2α reduction in excitatory neurons on translational landscape, we performed both excitatory neuron-specific translational profiling (RiboTag, Extended Data Fig. 4a–g) and general proteomic analysis in the dorsal hippocampus of *Eif2a* cKI^{Camk2a} and control (*Camk2a*-Cre^{+}) mice under basal conditions and following learning. Global correlation analysis showed that the translational changes in excitatory neurons caused by ablation of p-eIF2α were highly similar to learning-induced alterations ($R = 0.51$, $P < 0.0001$, Pearson correlation; Extended Data Fig. 5a, Supplementary Table 1). Moreover, changes in the general CA1 proteome caused by ablation of p-eIF2α were correlated with the changes induced by learning in control mice ($R = 0.49$, $P < 0.0001$, Pearson correlation; Extended Data Fig. 5b, Supplementary Table 1). Notably, the proteomic data showed differences in the levels of proteins related to axon guidance (CRMP1, DPYSL3, DPYSL4, DPYSL5, EPHB6, RAF1, RHOA; false-discovery rate (FDR)-adjusted $P < 0.05$) caused by both ablation of p-eIF2α and learning (Extended Data Fig. 5b, c).

p-eIF2α ablation in inhibitory neurons

Although modulation of protein synthesis in excitatory neurons is assumed to underlie memory consolidation[24], much less is known about the role of γ-aminobutyric acid-releasing (GABAergic) neurons in this process[25,26]. We ablated p-eIF2α in a broad population of inhibitory neurons by crossing *Eif2a*$^{A/A}$*fTg*$^{+}$ mice with mice expressing Cre

recombinase under the glutamic-acid decarboxylase 2 (*Gad2*, also known as *Gad65*) promoter (*Eif2a* cKI^{Gad2}; Extended Data Fig. 6a). *Eif2a* cKI^{Gad2} mice exhibited selective elimination of p-eIF2α in GAD2^{+} GABAergic neurons (Extended Data Fig. 6b–d, r). Next, we studied contextual and auditory fear memory in *Eif2a* cKI^{Gad2} mice. A weak training protocol induced normal STM (measured 1 h after training) in both *Eif2a* cKI^{Gad2} and control mice (*Eif2a*$^{A/A}$ *fTg*$^{+}$ and *Gad2*-Cre^{+}; Extended Data Fig. 6e, g). However, LTM for both contextual (*Eif2a* cKI^{Gad2}, 44.8 ± 2.53%; *Eif2a*$^{A/A}$ *fTg*$^{+}$, 35.28 ± 2.77%; *Gad2*-Cre^{+}, 30.95 ± 2.64%) and auditory fear (*Eif2a* cKI^{Gad2}, 53.82 ± 4.63%; *Eif2a*$^{A/A}$ *fTg*$^{+}$, 37.96 ± 3.18%; *Gad2*-Cre^{+}, 39.29 ± 2.14%) were enhanced 24 h after training in *Eif2a* cKI^{Gad2} mice (Extended Data Fig. 6f, h). Both groups spent a similar amount of time in the outer and the inner zones of the open field (Extended Data Fig. 6i), indicating no difference in anxiety. Together, these results demonstrate that depletion of p-eIF2α in all GABAergic neurons results in enhanced memory consolidation.

We next performed electrophysiological experiments to study the effect of p-eIF2α depletion in GABAergic neurons on synaptic plasticity in hippocampal CA1. *Eif2a* cKI^{Gad2} mice exhibited persistent synaptic potentiation (L-LTP) in response to 1 × HFS (weak stimulation), whereas control animals showed only short-lasting potentiation (E-LTP) (Extended Data Fig. 6j–m). Four trains of HFS elicited L-LTP in both *Eif2a* cKI^{Gad2} and control mice (Extended Data Fig. 6n, o). Notably, we found no changes in basal synaptic transmission in slices from *Eif2a* cKI^{Gad2} mice (as evident by unaltered input–output relationships and unchanged PPF; Extended Data Fig. 6p, q). These data demonstrate that a reduction in p-eIF2α in inhibitory neurons is sufficient to convert transient E-LTP into sustained L-LTP.

p-eIF2α ablation in SST^{+} neurons

In light of the finding that p-eIF2α is reduced in SST^{+} neurons following contextual learning (Extended Data Fig. 1e, h), it is conceivable that the effect of reduced p-eIF2α in GABAergic neurons on memory consolidation is mediated by SST^{+} neurons. SST^{+} neurons play a pivotal role in the regulation of neuronal circuits that underlie the formation of memory traces[26,27]. We therefore ablated p-eIF2α in SST^{+} neurons (*Eif2a*$^{A/A}$ *fTg*$^{+}$ *Sst*-Cre^{+}) as well as in PVALB^{+} neurons (*Eif2a*$^{A/A}$ *fTg*$^{+}$ *Pvalb*-Cre^{+}), which are another major population of inhibitory neurons (Fig. 2a, b, Extended Data Figs. 7a, b (*Eif2a* cKI^{Sst}), 8a–c (*Eif2a* cKI^{Pvalb})). Behavioural tests showed that contextual and cued fear memory was enhanced in *Eif2a* cKI^{Sst} mice (Fig. 2c, d) but not in *Eif2a* cKI^{Pvalb} mice (Extended Data Fig. 8d, e). *Eif2a* cKI^{Sst} and *Eif2a* cKI^{Pvalb} mice showed no changes in anxiety-like behaviours in an open field test (Extended Data Figs. 7e (*Eif2a* cKI^{Sst}), 8f (*Eif2a* cKI^{Pvalb})). The puromycin incorporation assay showed that basal protein synthesis was enhanced in SST-expressing neurons in *Eif2a* cKI^{Sst} mice (Extended Data Fig. 7c, d, increase of 47.1 ± 12.33%) and PVALB-expressing neurons in *Eif2a* cKI^{Pvalb} mice (Extended Data Fig. 8g, h, increase of 58.05 ± 8.86%).

Hippocampal CA1 synaptic plasticity was differentially altered in *Eif2a* cKI^{Sst} and *Eif2a* cKI^{Pvalb} mice. Weak stimulation (1 × HFS) elicited short-lasting E-LTP in slices from *Eif2a* cKI^{Pvalb} mice (Extended Data Fig. 9a–c), whereas this stimulation induced persistent L-LTP

in *Eif2a* cKI^{Sst} slices (Fig. 2e, f, Extended Data Fig. 7f). Both genotypes developed L-LTP in response to strong stimulation (4 × HFS) (Extended Data Figs. 7g, h (*Eif2a* cKI^{Sst}), 9d, e (*Eif2a* cKI^{Pvalb}). Whole-cell recordings from SST$^+$ neurons lacking p-eIF2α showed no change in their intrinsic properties or miniature excitatory synaptic inputs, but revealed a reduction in evoked firing (Fig. 2g–j, Extended Data Fig. 7i–m). Recordings from CA1 pyramidal neurons demonstrated that ablation of p-eIF2α in SST$^+$ interneurons reduced the amplitude of mIPSCs in pyramidal neurons (Fig. 2k–m). Recording from PVALB$^+$ interneurons lacking p-eIF2α showed a reduction in mEPSC amplitude and intact membrane properties (Extended Data Fig. 9f–i, m–r), but no change in miniature inhibitory synaptic inputs to pyramidal neurons (Extended Data Fig. 9j–l). These data demonstrate that although genetic reduction of p-eIF2α enhances translation in SST$^+$ and PVALB$^+$ neurons, the reduction of p-eIF2α only in SST$^+$ neurons, and not PVALB$^+$ neurons, enhances synaptic plasticity and memory consolidation.

CA1 SST$^+$ neurons—chiefly oriens-lacunosum moleculare (OLM) cells—are dendrite-projecting inhibitory interneurons that differentially regulate distal and proximal input pathways onto pyramidal cells. Via proximal disinhibition, they facilitate synaptic transmission and plasticity in the Schaffer collateral pathway; via distal inhibition, they inhibit synaptic transmission and plasticity in the temporoammonic pathway, which conveys inputs from the entorhinal cortex[28] (Extended Data Fig. 10a–c). To study the effect of reduced p-eIF2α in SST$^+$ neurons on the plasticity of inputs from the entorhinal cortex, we activated SST$^+$ neurons with theta-burst stimulation (TBS) in the oriens–alveus and examined the reduction in LTP (induced by weak TBS) in the temporoammonic pathway. LTP in this pathway was more suppressed in slices from *Eif2a* cKI^{Sst} mice than control *Sst*-Cre$^+$ mice (Extended Data Fig. 10d–f). Thus, a reduction in p-eIF2α in SST$^+$ neurons promotes memory formation via two mechanisms; first, it increases the responsiveness of pyramidal neurons to Schaffer collateral inputs by disinhibition and thereby facilitates LTP at these synapses; and second, it suppresses LTP at the temporoammonic pathway, thereby modulating sensory inputs from entorhinal cortex[28].

To corroborate the role of CA1 SST$^+$ neurons in memory consolidation by a different approach, we silenced CA1 SST$^+$ neurons using the inhibitory designer receptor exclusively activated by designer drug (DREADD) during the consolidation of fear memory. Silencing of SST$^+$ neurons attenuated contextual fear memory 24 h after training (Fig. 2o, p) with no effect on hippocampus-independent auditory cued fear memory (Extended Data Fig. 7n, o), demonstrating that hippocampal SST$^+$ GABAergic neurons are pivotal for memory consolidation.

Neuronal type-specific eIF2α mechanisms

Memory and consolidation of synaptic plasticity are defined biochemically as protein synthesis-dependent phenomena, which can be regulated by p-eIF2α or other signalling pathways such as the mammalian target of rapamycin complex 1 (mTORC1)[29]. Notably, the reduction in p-eIF2α in excitatory and inhibitory SST$^+$ neurons may exert its effect on memory and synaptic plasticity through an increase in general mRNA translation, a decrease

in translation of a subset of mRNAs that harbour upstream open reading frames (such as *Atf4*), or a combination of both.

We have identified the neuronal subtypes that enable p-eIF2α-dependent consolidation of memory and measured the effect of p-eIF2α elimination in specific cell types in the dorsal hippocampus on intrinsic, synaptic, circuit and behavioural phenotypes. Reduced p-eIF2α in excitatory neurons promotes L-LTP and long-term memory formation via an increase in excitatory and a decrease in inhibitory synaptic inputs. The decrease in inhibitory synaptic transmission could be mediated via protein synthesis-dependent trans-synaptic mechanisms[30].

This study shows that a reduction in p-eIF2α specifically in excitatory neurons has effects on L-LTP and long-term memory. Moreover, we have identified autonomous p-eIF2α-dependent mRNA translation mechanisms that regulate memory consolidation and are mediated by SST^+ neurons, which have been strongly implicated in contextual memory[27], cued fear memory[31], and motor learning[32]. The ablation of p-eIF2α in SST^+ interneurons may promote memory by reducing inhibitory synaptic inputs onto pyramidal neurons, lowering the threshold for L-LTP induction, and repressing the flow of sensory information from the entorhinal cortex by suppressing potentiation of the temporoammonic pathway (Extended Data Fig. 10g–i).

The existence of two autonomous memory consolidation processes mediated by p-eIF2α-dependent translational control in excitatory and SST^+ neurons might impart an evolutionary advantage in ensuring and regulating the endurance of a given memory trace. Notably, these two processes appear to be complementary: translational changes in excitatory neurons help to facilitate memory consolidation by modulating synaptic plasticity in a sparse population of CA1 pyramidal neurons, whereas translational changes in SST^+ inhibitory neurons facilitate memory consolidation by gating synaptic plasticity in the CA1 circuit.

Methods

Animals and environment

Neuronal subtype-specific eIF2α conditional knock-in (cKI) mice were generated by breeding $Eif2a^{A/A}fTg^+$ floxed mice[19] with a Cre^+ transgenic line driven by the *Camk2a*, *Gad2*, *Pvalb*, or *Sst* promoters. The genetic background of these strains is C57BL/6. We first bred $Eif2a^{A/A}fTg^+$ mice with neuronal subtype-specific Cre mice to generate Cre-positive, $Eif2a^{A/S}fTg^+$ heterozygous mice. $Eif2a^{A/S}fTg^+$-Cre^+ mice were then bred with $Eif2a^{A/A}fTg^+$ mice to generate homozygous *Eif2a* cKI mice and Cre-negative, $Eif2a^{A/A}fTg^+$ or neuronal subtype-specific X-Cre^+ control mice (Supplementary Table 2). Adult (2–3 months old, weight 26–30 g) male mice were used. Mice were housed in standard laboratory cages with 4–5 mice in each cage and kept on a 12-h light (between 7:00 a.m. and 7:00 p.m.), 12-h dark cycle. Mice were given water and standard rodent chow ad libitum. Cages were maintained in ventilated racks in temperature- (20–21 °C) and humidity- (~55%) controlled rooms. Mice were maintained under standard conditions at the Goodman Cancer Research Centre (GCRC) animal facility, and all experiments were carried out under the Canadian Council on Animal Care (CCAC) guidelines and were approved by both McGill University and the

University of Montréal. The experiments were conducted only during the light phase of the cycle and the experimenter was blind to the genotype for all behavioural tests. The experiments were not randomized. Mice were anaesthetized with isoflurane before the surgical procedures. For euthanasia, animals were exposed to carbon dioxide as per CCAC guideline recommendations followed by cervical dislocation. No statistical methods were used to predetermine sample size.

Stereotaxic surgery

Infusion of AAV into adult mouse brain—For virus infusion, anaesthesia was induced with 3% isoflurane and maintained with 1.5% isoflurane. Mice were mounted on a Kopf stereotaxic frame, a midline incision was made, and the skull was exposed, allowing a small hole to be drilled above the hippocampus of each hemisphere. Using a 5-μl Hamilton syringe with a 23-gauge needle attached to a stereotactic infusion pump, mice received 0.5 μl of AAV expressing AAV9.*Camk2a*0.4.Cre.SV40 (2.8×10^{13} genome copies per ml (GC/ml)), AAV9.*Camk2a*0.4.eGFP.WPRE.rBG (3.49×10^{13} GC/ml), AAV9-EF1α-DIO-EYFP-WPRE-hGH (4.2×10^{12} GC/ml) or AAV-EF1α-DIO-Rpl22–3HA-IRES-YFP-WPRE (7.0×10^{12} GC/ml) over 10 min per hemisphere, for the CA1 (anteroposterior, −1.90 mm relative to bregma; lateral, ± 1.0 mm; ventral, −1.50 mm) and for the amygdala (anteroposterior, −1.22 mm relative to bregma; lateral, ± 2.9 mm; ventral, −4.50 mm) according to the Franklin and Paxinos atlas[33]. The needle was kept in place for 5 min before and after infusion to minimize fluid retraction. The mice were allowed at least 3 weeks to recover from surgery before any behavioural experiments were conducted.

Cannula implantation and microinjection of puromycin—Anaesthetized mice were bilaterally implanted with an infused guiding cannula into the CA1 region (anteroposterior, −1.90 mm relative to bregma; lateral, ± 1.0 mm; ventral, −1.0 mm), secured in place by dental cement. The guiding cannula was fitted with a 28-gauge dummy cannula that prevents blockage. Mice were given one week to recover after surgery before infusion of puromycin. Mice were infused with puromycin dissolved in dimethyl sulfoxide (DMSO) and further diluted in saline to a final DMSO concentration of 0.1%, via a 28-gauge infusion cannula. The infusion cannula protruded 0.25 mm beyond the guide cannula. After infusion, the injection cannula was kept in the guide cannula for an additional minute to minimize dragging of infused solutes along the injection tract.

In vivo surface labelling of translation (iSUnSET)

For in vivo iSUnSET labelling, CA1-cannulated mice were infused with 5 μg/μl puromycin. Thirty minutes after injections, mice were anaesthetized and perfused with 0.1 M phosphate buffer (PB) followed by 4% paraformaldehyde (PFA) in PB. Perfused brains were fixed overnight in 4% PFA and cryoprotected sequentially in 20 ml of 10%, 20%, and 30% sucrose in phosphate-buffered saline (PBS) at 4 °C. Puromycin incorporation was determined using anti-puromycin antibody and co-stained with PVALB or SST antibodies (Supplementary Table 3a, b). Slices were imaged with a confocal microscope (Zeiss LSM 800) and processed using ImageJ (NIH).

Fluorescent non-canonical amino-acid tagging (FUNCAT) and immunolabelling

The mice were fed with a low-methionine diet for 1 week before fear conditioning and azidohomoalanine (AHA) injection. The non-canonical amino acid AHA was diluted in PBS, pH 7.4 and 100 μg/g AHA was injected intraperitoneally (i.p.) after strong fear conditioning training (two pairings of 2,800 Hz, 85 dB, 30 s tone with 0.7 mA, 2 s foot shock). Mice were anaesthetized 180 min after the AHA injection, and transcardially perfused with PBS. Free-floating dorsal hippocampus sections (40 μm thick) were incubated overnight at 4 °C in blocking solution (0.5% Triton-X100 and 10% goat serum in PBS and 5% sucrose). Sections were extensively washed, and 'clicked' overnight with 2 μM fluorescent Alexa Fluor 555 alkyne (Supplementary Table 3) in click buffer composed of 200 μM triazole ligand, 400 μM TCEP and 200 μM $CuSO_4$ in PBS. After incubation, slices were washed in PBS/Triton followed by three rinses in PBS at room temperature, and mounted on microscope slides. Confocal images were analysed using ImageJ. The AHA incorporation and fluorescent signal were significantly reduced in the presence of the protein synthesis inhibitor anisomycin or in the absence of the copper catalyst (data not shown).

CNO administration

For in vivo silencing of neurons expressing AAV9-DIO-hM4D(Gi)-mCherry (hM4Di; 2.5×10^{13} GC/ml) in mice, CNO was dissolved in 100% DMSO and diluted with 0.9% saline to a final dose of 1 mg kg^{-1} CNO in 0.001% DMSO. To silence hM4Di-expressing neurons, CNO was injected i.p. immediately after the acquisition of fear conditioning.

Field potential recordings

Male mice (2–3 months old) were anaesthetized with isoflurane and the brain was rapidly excised and placed in an ice-cold sucrose-based cutting solution saturated with 95% O_2 and 5% CO_2 containing (in mM): 87 NaCl, 2.5 KCl, 1.25 NaH_2PO_4, 7 $MgSO_4$, 0.5 $CaCl_2$, 25 $NaHCO_3$, 25 glucose, 11.6 ascorbic acid, 3.1 pyruvic acid, and 75 sucrose, pH 7.4, and 295 mOsmol. Transverse hippocampal slices (400 μm thickness) were prepared and allowed to recover for at least 1 h at 30 °C submerged in oxygenated artificial cerebrospinal fluid (ACSF; 124 mM NaCl, 2.5 mM KCl, 1.25 mM NaH_2PO_4, 1.3 mM $MgSO_4$, 2.5 mM $CaCl_2$, 26 mM $NaHCO_3$, and 10 mM glucose). Individual slices were perfused with ACSF for an additional 30 min in a recording chamber at 27–28 °C. Field EPSPs (fEPSPs) were recorded in CA1 stratum radiatum with glass electrodes (2–3 MΩ) filled with ASCF. Independent Schaffer collateral fEPSPs were evoked using two concentric bipolar tungsten stimulating electrodes placed in mid-stratum radiatum on either side of the recording electrode. Baseline stimulation was applied alternatively to the two pathways at 0.033 Hz by delivering 0.1-ms pulses, with intensity adjusted to evoke fEPSPs with 30% maximal amplitude. Early phase long-term potentiation (E-LTP) was induced by one train of 0.1 ms pulses at high-frequency stimulation (1 × HFS, 100 Hz) for 1 s and was analysed 30 min after HFS. For L-LTP, the HFS train was repeated four times at 5-min intervals and LTP was measured 180 min after the last HFS. For the LTP in temporoammonic–CA1 pathway experiments, a concentric stimulation electrode was positioned at the oriens–alveus (O/A) border to evoke LTP in O/A region neurons using a theta-burst stimulation (TBS) paradigm consisting of five bursts (four stimuli at 100 Hz with 250-ms inter-burst interval) delivered at 5 Hz, repeated three times at

an interval of 30 s. The temporoammonic (TA) pathway was stimulated by a brief (0.1 ms) electrical stimulation delivered every 30 s in the stratum lacunosum-moleculare (SLM) region in CA1. After 30 min of stable baseline in the presence or absence of TBS in the O/A region, TA-LTP was induced using a weak theta-burst stimulation (wTBS) consisting of two bursts (four stimuli at 100 Hz) delivered at a 200-ms interval. Stimulation intensity and duration were constant throughout the entire experiment, including the wTBS induction protocol. fEPSP slope measurements were performed on digitized analogue recordings using the Clampfit analysis function. The slope was measured between 10% and 90% of maximal fEPSP amplitude during an epoch defined by constant cursor placements, which excluded fibre volley and population spikes.

Whole-cell recording

Whole-cell patch clamp recordings were obtained from CA1 pyramidal, $PVALB^+$ and SST^+ neurons under visual guidance with eGFP expression, using a borosilicate glass pipette (3–5 MΩ; WPI). For whole-cell voltage-clamp, the intracellular solution contained the following (in mM): 120 $CsMeSO_3$, 5 CsCl, 2 $MgCl_2$, 10 HEPES, 0.5 EGTA, 10 Na_2-phosphocreatine, 2 ATP-Tris, 0.4 GTP-Tris, 0.1 spermine, 2 QX-314 (pH 7.2–7.3; 280 ± 5 mOsmol/l). For whole-cell current-clamp, borosilicate glass pipettes were filled with an internal solution containing (in mM) 120 $KMeSO_4$, 10 KCl, 10 HEPES, 0.5 EGTA, 10 Na_2-phosphocreatine, 2.5 MgATP, 0.3 NaGTP (pH 7.4; 300 mOsmol/l). The oxygenated ACSF contained the following (in mM): 124 mM NaCl, 5 mM KCl, 1.25 mM NaH_2PO_4, 2 mM $MgSO_4$, 2 mM $CaCl_2$, 26 mM $NaHCO_3$, and 10 mM glucose. Data were collected with multiclamp 700A or 700B amplifiers (Molecular Devices), and digitized at 20 kHz using Digidata 1440A and pClamp 10 (Molecular Devices). Recordings were low-pass filtered at 2 kHz. Access resistance (15–25 MΩ) was regularly monitored during experiments and data were included only if the holding current was stable and access resistance varied by less than 20% of initial value. mEPSCs were recorded at −70 mV in the presence of SR-95531 (gabazine; 5 μM, Sigma), (2R)-amino-5-phosphonovaleric acid (AP5; 50 μM, Sigma, St-Louis, MO) and tetrodotoxin (TTX; 1 μM, Abcam). For mIPSCs, cells were recorded at 0 mV and gabazine was replaced by 6-cyano-7-nitroquinoxaline-2,3-dione (CNQX; 20 μM, Sigma, St-Louis, MO). mEPSCs and mIPSCs were recorded over a period of 10–20 min; 200–300 (mEPSCs) and 300 (mIPSCs) consecutive events were analysed for frequency and amplitude (MiniAnalysis, Synaptosoft, Fort Lee, NJ). The firing properties of pyramidal, $PVALB^+$ and SST^+ neurons were measured in current-clamp mode recording[34,35]. Resting membrane potential (RMP) was measured directly after breaking the membrane. Input resistance (*R*in) was measured using a linear regression of voltage deflections (±15–25 mV) in response to current steps (800 ms, 20 pA increment for pyramidal neurons, and $PVALB^+$ interneurons; 500 ms, 20 pA increment for SST^+ interneurons; at holding potential of −70 mV). The firing frequency–current gain (*F*–*I*) relationship was measured from the number of action potentials evoked by somatic current injections of increasing intensity (0–400 pA, 20 pA steps, 500–800 ms duration). Linear regressions were applied to individual *F*/*I* curves and the neuronal gain, defined as the slope of the *F*/*I* curve, was calculated.

Open field test

Animals were first habituated to the dimly lit experimental room (~15 lx) for 30 min and then individually placed in an illuminated clear Plexiglas chamber (50 × 50 × 50 cm, ~1,200 lx) with a white floor. Animals were allowed to explore freely for 10 min following an initial 1-min habituation phase. Total path length was calculated using EthoVision XT-12 video tracking software (Noldus Information Technology, USA).

Fear conditioning

Prior to the experiment, mice were handled for 5 min per day for three consecutive days. Habituation was done by exposing mice to two distinct contexts; context A (grid floor with transparent cage walls) and context B (grid floor and cage walls were covered with yellow plastic to create another context) for 20 min for 2 days. The two habituation sessions were separated by at least 4 h. During training, mice explored context A for 2 min, then received one pairing of a tone (sound-1, frequency 2,800 Hz and amplitude 85 dB for 30 s) co-terminated with a foot shock (0.35 mA, 1 s) in the weak training protocol or two pairings of a tone (2,800 Hz, 85 dB, 30 s) with a co-terminating foot shock (0.7 mA, 2 s) for the strong training protocol. Sixty seconds later, they were returned to their home cage. Contextual fear was tested 1 h (STM) and 24 h (LTM) after conditioning by placing the animals in the conditioning context (context A) for a 5-min period, and time spent freezing was used as an indicator of fear learning and memory. For auditory fear conditioning, the test consisted of a 2-min acclimatizing period to the context (context B; pre-CS period), followed by a 3-min period during which the tone was delivered (CS). Mice were returned to their cages 30 s after the end of the tone. For all tests, each mouse was assessed at 5-s intervals as either freezing or not freezing. Data are expressed as the percentage of 5-s intervals in which freezing was observed. Statistical analysis was based on repeated measures ANOVA and between-group comparisons by Tukey’s post-hoc test.

Immunohistochemistry and image analysis

Mouse brains were fixed by transcardial perfusion with 0.1 M PB and 4% PFA in PB followed by 24 h of post-fixation in the same solution at 4 °C. Whole brains were cryoprotected sequentially in 20 ml of 10%, 20%, and 30% sucrose in PBS at 4 °C. Cryostat sections (40 μm thickness) were blocked in 20% normal goat serum (NGS) containing 0.1% Triton-X100 and incubated overnight with primary antibodies diluted in 2% NGS in PBS at 4 °C, rinsed three times for 10 min in PBS and finally incubated with secondary antibodies diluted in 2% NGS in PBS for 1 h at room temperature. Slices were then rinsed three times for 10 min in PBS before being mounted on slides using SlowFade Gold antifade mountant (Thermo Fisher Scientific, USA). Primary and secondary antibodies are listed in Supplementary Table 3. The slices were imaged with a confocal microscope (Zeiss LSM 800). Image processing was performed with ImageJ (NIH).

Sample preparation and LC–MS/MS analysis

Tissues were flash frozen and shipped on dry ice to Cell Signaling Technology for analysis. Tissues were thawed in urea lysis buffer (9M urea, 20 mM HEPES pH 8.0, 2× phosphatase inhibitor cocktail (CST #5870)), homogenized, sonicated, centrifuged, reduced with DTT,

and alkylated with iodoacetamide. One hundred micrograms of each sample was digested with LysC followed by trypsin, reverse-phase purified over C18 SEP PAK columns (Waters), labelled with TMT 10-plex reagent (Thermo), bRP fractionated (96 fractions concatenated non-sequentially to 12), C18 purified for liquid chromatography with tandem mass spectrometry (LC–MS/MS) and used for total proteome analysis as previously described[36]. LC–MS/MS analysis was performed using an Orbitrap-Fusion Lumos Tribrid Mass spectrometer as previously described[36,37]. Peptides were separated using a 50 cm × 100 μM PicoFrit capillary column packed with C18 reversed-phase resin and eluted with a 150-min linear gradient of acetonitrile in 0.125% formic acid delivered at 280 nl/min. For total proteome analysis, an MS3 method was used to reduce ion interference and ratio compression. MS3 parameters: method duration 210 min, user-defined lock mass 371.10123, Orbitrap resolution 120K, scan range 350–1,400 *m*/*z*, maximum injection time 100 ms, AGC target 5×10^5, dynamic exclusion 1, exclusion duration 120 s, mass tolerance ±7 ppm, MS2 isolation mode quadrupole, MS2 isolation window 0.4, activation type CID, collision energy mode fixed, collision energy 35, detector type IonTrap, max injection time 10 ms, AGC target 2×10^4, MS3 isolation mode quadrupole, isolation window 0.7, multi-notch isolation, MS2 isolation window 3 *m*/*z*, number of notches 10, collision energy mode fixed, collision energy 65, detector type Orbitrap, Orbitrap resolution 50K, max injection time 150 ms, AGC target 2.5×10^5.

Peptide and protein identification

MS spectra were evaluated by Cell Signaling Technology using SEQUEST and the GFY-Core platform (Harvard University)[38,39,40]. Searches were performed against the most recent update of the Uniprot *Mus musculus* database (20190703 update) with a mass accuracy of ±50 ppm for precursor ions and 0.02 Da for productions. Cysteine carboxamidomethylation was specified as a static modification (C + 57.02146374) as was TMT labelling of lysine (K + 229.162932) and TMT labelling of N termini (Nterm + 229.162932). Oxidation of methionine (M + 15.9949146221) was specified as a variable modification. Results were filtered to a 1% peptide-level false discovery rate (FDR) and further filtered to a 1% protein level FDR. TMT quantitative results were generated in GFY-Core based on reporter ion signal to noise values in each channel. Individual peptide signal to noise values were summed for each protein, and relative protein abundance between channels was compared. *P* values were based on a two-tailed *t*-test across replicates.

RiboTag assays, RNA sequencing library preparation and analysis

Frozen hippocampi from one mouse were pooled and homogenized in 1 ml buffer as described[41]. After centrifugation, 4 μl anti-HA antibody (Supplementary Table 3) was added to 800 μl cleared lysate and incubated for 4 h at 4 °C. The remaining lysate was saved as input sample. After incubation, 200 μl protein A/G magnetic beads (Thermo Fisher Scientific) was added and incubated overnight at 4 °C with rotation. Immunoprecipitates (IPs) were washed in high-salt buffer and RNA from inputs and IPs extracted as described in the original protocol[42]. RNA-seq libraries were prepared from 200 ng total RNA using the NEBNext Ultra II Directional RNA Library Prep Kit for Illumina with the NEBNext Poly(A) mRNA Magnetic Isolation Module and NEBNext Multiplex Oligos (New England Biolabs). Libraries were pair-end sequenced (2 × 50 bp) on an Illumina NovaSeq Instrument.

The adaptor sequence GATCGGAAGAGCACACG was removed from reads using Cutadapt. Reads shorter than 25 nucleotides were discarded. Reads were aligned to ribosomal RNA using Bowtie[43], allowing for two mismatches and no ambiguous mapping, and aligned reads were discarded. The remaining forward pair reads were then aligned to the mouse transcriptome (Gencode version 14) using Bowtie, allowing for two mismatches and no ambiguous mapping[43,44]. Differential expression analysis was carried out using DESeq2 version 1.26.0[45]. To examine a global correlation between the effect of ablation of p-eIF2α and learning, we calculated Pearson correlations between $\log_2$ fold change values. The Pearson correlation and significance test were done using R. Functional enrichment analysis for subsets of transcripts or proteins was calculated using Enricher tool (EnrichR)[46]. Enrichment was considered significant for FDR-adjusted *P* values <0.1. The full dataset of the RiboTag gene-expression data is available at the National Centre for Biotechnology Information Gene Expression Omnibus (GEO accession number GSE152825).

Statistical analysis

Data are presented as mean ± s.e.m. The statistical tests were performed using GraphPad Prism 7.00 (GraphPad Prism Software Inc., USA). The statistical significance of differences between two groups was determined using two-tailed unpaired Student's *t*-test with Welch's correction. Multiple groups were compared by one-way ANOVA or two-way ANOVA. The statistical significance differences at different time points were determined using a two-way repeated measure ANOVA or mixed-effects model (REML). The post-hoc test (Tukey's or Sidak's, α level of 0.05 and $P < 0.05$) used to compare individual groups is indicated in the figure legends. All statistical comparisons are listed in Supplementary Table 4.

Reporting summary

Further information on research design is available in the Nature Research Reporting Summary linked to this paper.

Data availability

The full RiboTag gene-expression dataset is available at the National Centre for Biotechnology Information Gene Expression Omnibus (GEO accession number GSE152825). The additional relevant data that support the findings of this study are available from the corresponding author upon reasonable request. Source data are provided with this paper.

Extended Data

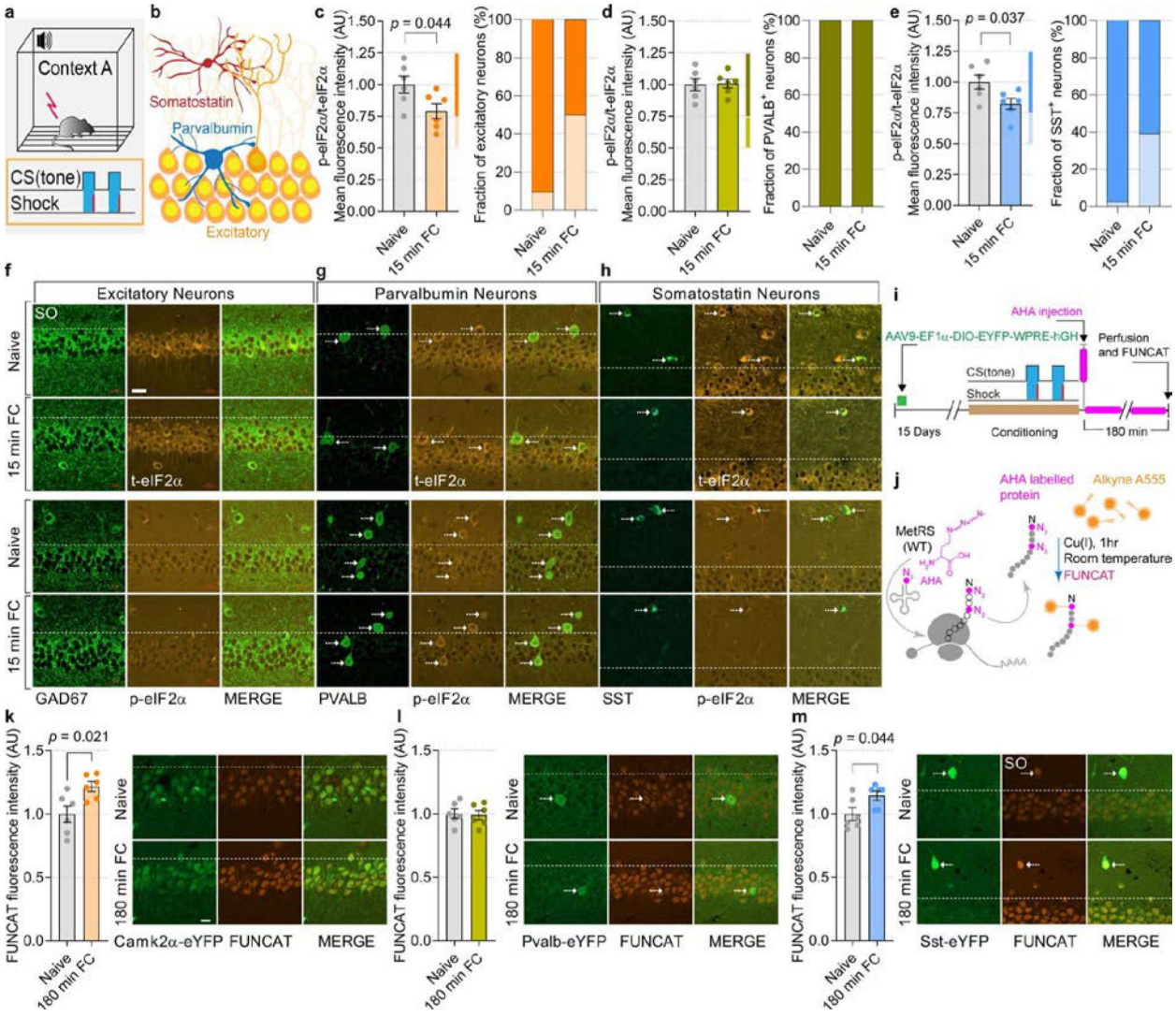

Extended Data Fig. 1. Learning-induced reduction of p-eIF2α levels in excitatory and in the SST-expressing sub-population of GABAergic neurons.

a, Schematics of the fear conditioning experiment. **b**, Illustration of different neuronal subtypes in the CA1 region of the hippocampus. **c**, Quantitative analyses of immunofluorescence images depicting levels of p-eIF2α in CA1 excitatory neurons 15 min after fear conditioning. In the CA1 region, fear conditioning significantly reduces p-eIF2α in excitatory neurons ($t_{9.8} = 2.31$; $n = 6, 6, 12$ neurons per 67,600 μm^2 of mouse CA1). Graph on the right depicts a fraction of excitatory neurons showing a decrease in p-eIF2α (between 25–50% decrease) after fear conditioning. **d**, The p-eIF2α levels in CA1 PVALB$^+$ neurons remain unchanged 15 min after fear conditioning ($t_{9.17} = 0.112$; $n = 6, 6, 10–11$ neurons per 84,500 μm^2 of mouse CA1). **e**, The fear conditioning significantly reduces p-eIF2α in the CA1 SST$^+$ neurons ($t_{9.44} = 2.43$; $n = 6, 6, 6–7$ neurons per 84,500 μm^2 of mouse CA1). Graph on the right shows that in 39.02% of CA1 SST$^+$ neurons, fear conditioning causes 25–50% decrease in p-eIF2α levels. **f**–**h**, Representative images of p-eIF2α levels in

excitatory (GAD67-negative neurons in CA1 pyramidal layer) and GABAergic neurons (PVALB- and SST-expressing) in naive and fear conditioning mice. Three independent experiments showed similar results. **i**, Timeline for fluorescent labelling of specific neuronal subtypes in CA1, fear conditioning paradigm and AHA injections to identify newly synthesized proteins. **j**, To visualize AHA-labelled proteins, the azide group (pink) of AHA is covalently bonded with fluorescent alkyne group (orange) through Cu(I) mediated fluorescent non-canonical amino acid tagging (FUNCAT). **k**, A 21.67 ± 3.91% increase in protein synthesis was observed in the CA1 excitatory neurons of fear conditioning compared to naive mice using FUNCAT ($t_{8.14}$ = 2.85; n = 6, 6, 12 neurons per mouse). Representative images of CA1 excitatory neurons showing FUNCAT in naive and fear conditioning mice. Two independent experiments showed similar results. **l**, Fear conditioning does not affect general protein synthesis in CA1 PVALB$^+$ neurons ($t_{9.99}$ = 0.23; n = 6, 6, 6 neurons per mouse). Representative images of GABAergic PVALB$^+$ neurons with FUNCAT. Two independent experiments showed similar results. **m**, In the CA1 SST$^+$ neurons, fear conditioning causes 14.33 ± 3.64% increase in AHA labelling and FUNCAT signal intensity ($t_{9.09}$ = 2.33; n = 6, 6, 5 neurons per mouse). Representative images of CA1 GABAergic SST-expressing neurons with FUNCAT in naive and fear conditioning mice. Two independent experiments showed similar results. Stratum oriens (S.O.). Data are presented as mean ± s.e.m. in **c**–**e**, **k**–**m**. p-values by two-tailed unpaired t-test with Welch's correction in **c**, **e**, **k** and **m** are indicated. Points represent individual mice. Scale bars: 20 μm.

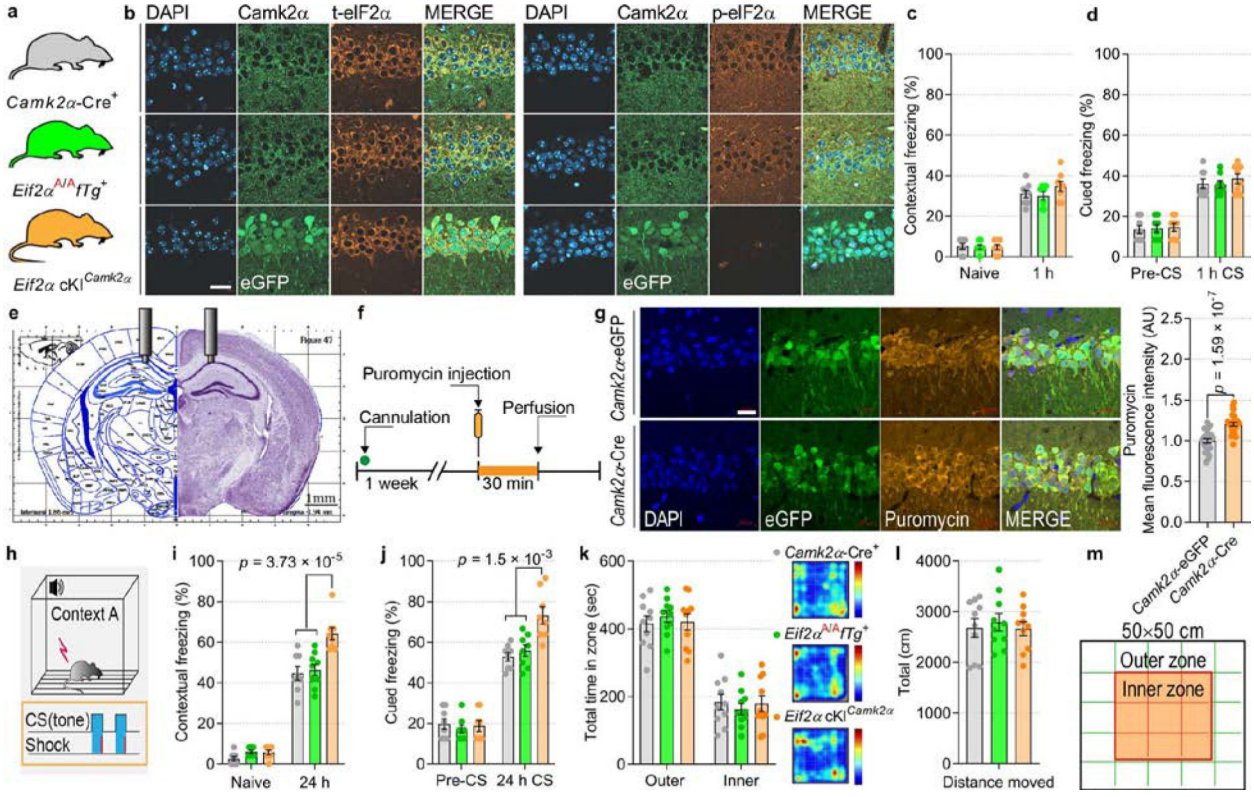

Extended Data Fig. 2. *Eif2a* cKI^{Camk2a} mice show enhanced protein synthesis and consolidation of contextual and auditory fear memory.

a, **b**, Immunofluorescent labelling of excitatory neurons shows a decrease in p-eIF2α levels in *Eif2a* cKI^{Camk2a} compared to control mice. Two independent experiments showed similar results. **c**, Short-term contextual memory is not altered in *Eif2a* cKI^{Camk2a} mice ($F_{2, 40}$ = 0.97; n = 8, 7, 8). **d**, Short-term auditory fear memory is not altered in *Eif2a* cKI^{Camk2a} mice ($F_{2, 42}$ = 0.46; n = 8, 8, 8). **e**, Illustration of cannulation site for unilateral injections of puromycin into the CA1 region. **f**, Experimental design of iSUnSET assay. **g**, Immunofluorescent images of puromycin in *Eif2a*$^{A/A}$ *fTg*$^{+}$ mice injected with AAV9.*Camk2a*0.4.Cre.SV40 (*Camk2a*-Cre) shows enhanced protein synthesis ($t_{50.43}$ = 6.08; n = 26, 27, points represent group means). Five independent experiments showed similar results. **h**, Schematic representation of strong contextual and auditory fear conditioning. **i**, Contextual memory is enhanced in *Eif2a* cKI^{Camk2a} mice following a strong training protocol ($F_{2, 44}$ = 12.97; n = 8, 9, 8). **j**, Auditory fear memory is enhanced in *Eif2a* cKI^{Camk2a} mice following a strong training protocol ($F_{2, 42}$ = 7.64; n = 8, 8, 8). **k**, In an open field test, all groups spent a similar amount of time in the outer and inner zones ($F_{2, 54}$ = 5.6 × 10^{-12}; n = 10, 10, 10). Representative heat-map of travelled path in an open field arena. **l**, The mean total distance moved (in cm) in the open field was similar in all groups ($F_{2, 27}$ = 0.19; n = 10, 10, 10). **m**, Open field test arena with illustration of outer and inner zones. Data are presented as mean ± s.e.m. in **c**, **d**, **g**, **i**–**l**. p-values by two-tailed unpaired t-test with Welch's correction in **g** and by two-way ANOVA in **i** and **j** followed by Tukey's multiple comparisons post hoc test are indicated. Points represent individual mice. Scale bars: 20 μm.

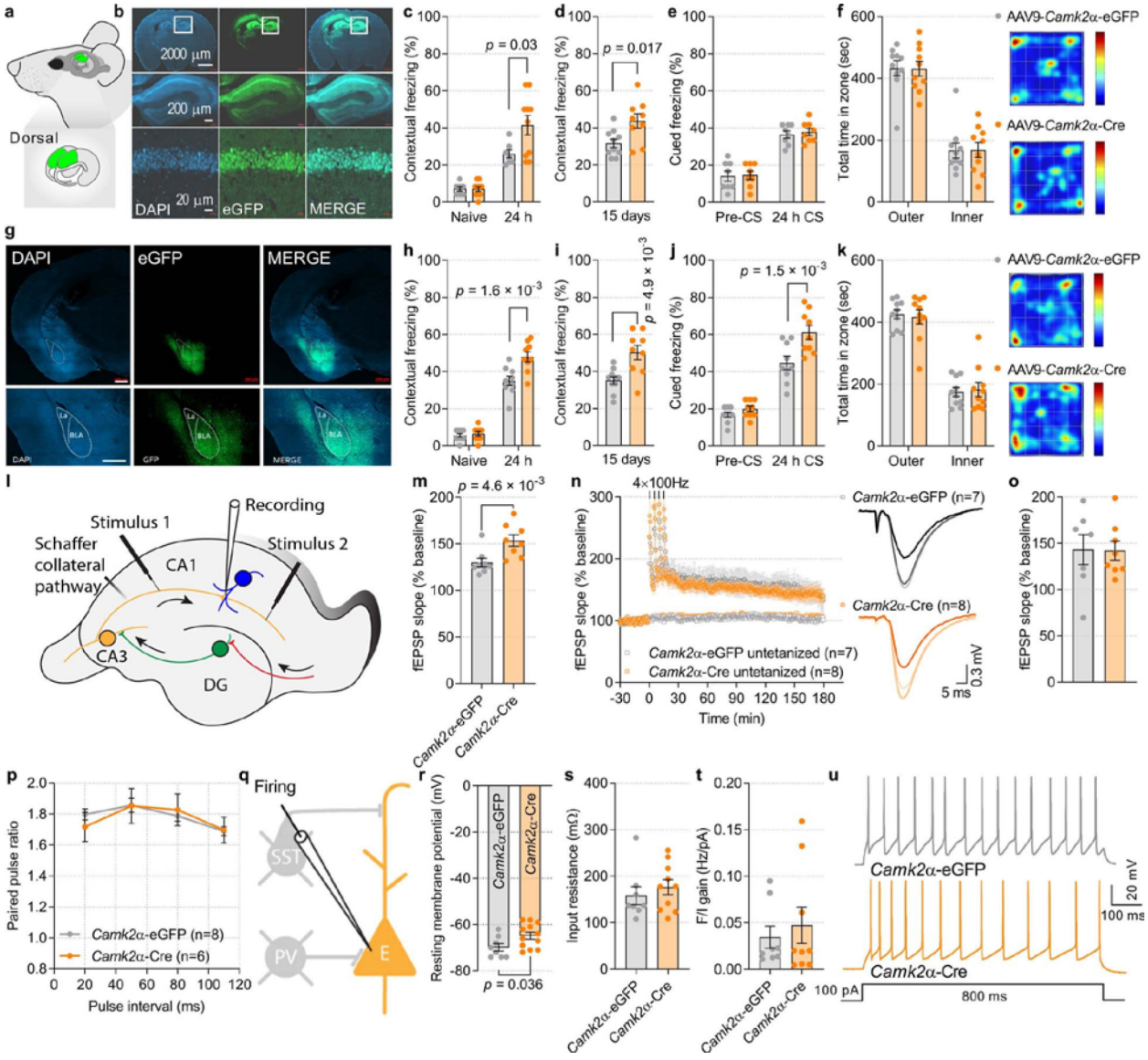

Extended Data Fig. 3. CA1- or amygdala-specific reduction of p-eIF2α facilitates consolidation of contextual fear memory.

a, Representative illustration of target area for p-eIF2α reduction in the dorsal hippocampus. Two independent experiments showed similar results. **b**, Immunohistochemistry for eGFP reporter demonstrates that deletion of WT *Eif2a fTg* is restricted to the CA1 region of the hippocampus. Two independent experiments showed similar results. **c**, **d**, *Eif2a*$^{A/A}$*fTg*$^{+}$ mice were injected with AAV9.*Camk2a*0.4.Cre.SV40 (AAV9-*Camk2a*-Cre) or control AAV9.*Camk2a*0.4.eGFP.WPRE.rBG (AAV9-*Camk2a*-eGFP) targeting the CA1. Contextual memory was significantly enhanced in AAV9-*Camk2a*-Cre-injected mice as compared to AAV9-*Camk2a*-eGFP-injected mice tested 24 h ($F_{1, 30} = 5.19$; $n = 7, 10$) and 15 days ($t_{13.19} = 2.72$; $n = 10, 9$) after training. **e**, Auditory fear memory remains unaffected ($F_{1, 28} = 0.18$; $n = 8, 8$). **f**, There was no difference in the time spent in the outer and inner zone in an open field test ($F_{1, 36} = 3.63 \times 10^{-9}$; $n = 10, 10$). Heat-map represents the group-average of path travelled in an open field arena, red = more time, blue = less time. **g**, Representative

immunohistochemistry images demonstrating the amygdala-specific injections of the virus. Scale bars: 500 μm. Two independent experiments showed similar results. **h**, **i**, Contextual memory was significantly enhanced in *Eif2a*$^{A/A}$*fTg*$^{+}$ mice injected with a virus expressing AAV9-*Camk2a*-Cre in the amygdala tested 24 h ($F_{1, 32} = 11.92$; $n = 9, 9$) and 15 days ($t_{12.2} = 3.42$; $n = 10, 9$) after training. **j**, Auditory fear memory is also enhanced ($F_{1, 32} = 12.01$; $n = 9, 9$). **k**, There was no difference in the time spent in the outer versus inner zone in an open field test ($F_{1, 36} = 8.3 \times 10^{-9}$; $n = 10, 10$). Heat-map represents the group-average of path travelled in an open field arena. **l**, Experimental scheme in acute hippocampal slices: Schaffer collateral fibres were stimulated in two independent pathways with extracellular electrodes and fEPSPs were recorded in CA1 stratum radiatum. **m**, A single high-frequency train (1 × HFS for 1 s) elicited early LTP in slices from AAV9.*Camk2a*0.4.eGFP.WPRE.rBG (*Camk2a*-eGFP)-injected mice (E-LTP 30 min post-HFS, $F_{1, 7} = 8.2$; $n = 8, 8$). **n**, **o**, L-LTP induced by four tetanic trains at 100 Hz is similar in slices from *Camk2a*-eGFP- and *Camk2a*-Cre-injected mice (**o**; $F_{1, 7} = 0.071$; $n = 7, 8$). **p**, Paired-pulse facilitation (PPF) is defined as the ratio of the amplitude of the 2nd versus the 1st fEPSPs responses over increasing time intervals. The decay rates of PPF did not differ between *Camk2a*-eGFP- and *Camk2a*-Cre-injected mice, indicating intact short-term plasticity ($F_{1, 48} = 0.041$; $n_{mice} = 8, 6$, points represent group means). **q**, Diagram of experimental arrangement for recording intrinsic and firing properties in CA1 excitatory neurons. **r**, Resting membrane potential was significantly increased in *Camk2a*-Cre-injected mice ($t_{16.59} = 2.28$; $n = 8, 12$). **s**, Input resistance is not affected in CAMK2α-eGFP and CAMK2α-Cre positive neurons ($t_{14.63} = 0.72$; $n = 8, 10$). **t**, The number of action potential in response to incremental somatic depolarization (F/I gain relationship) is not different between CAMK2α-eGFP^{+} and CAMK2α-Cre^{+} excitatory neurons ($t_{13} = 0.56$; $n = 8, 9$). **u**, Examples of traces obtained in response to 100 pA current injection in CAMK2α-eGFP^{+} or the CAMK2α-Cre^{+} excitatory neurons. Data are presented as mean ± s.e.m. in **c**–**f**, **h**–**k**, **m**–**p**, **r**–**t**. *p*-values by two-way ANOVA in **c**, **h**, **j**, followed by Sidak's multiple comparisons post hoc test; two-tailed unpaired *t*-test with Welch's correction in **d**, **i**, **r**; two-way ANOVA (repeated measurements) in **m** followed by Sidak's multiple comparisons post hoc test are indicated. Points represent individual mice unless stated otherwise.

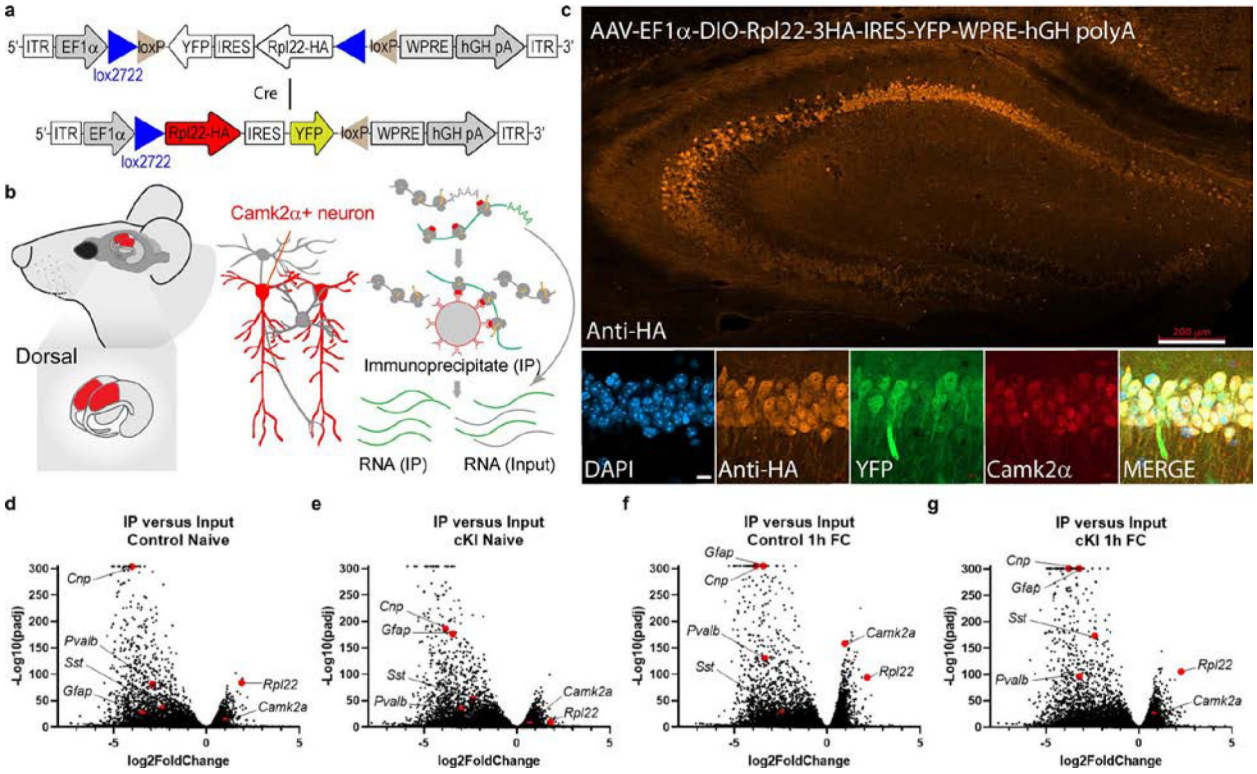

Extended Data Fig. 4. RiboTag.

a, Schematic representation of the AAV-EF1α-DIO-Rpl22–3HA-IRES-YFP-WPRE-hGH polyA (AAV-DIO-RiboTag) viral vector. We developed a Cre-dependent RiboTag viral vector based on AAV-DIO-RiboTag41. In the presence of Cre recombinase under a *Camk2a* promoter, the *Rpl22-HA-IRES-YFP* cassette is rearranged to the ON configuration that allows the Rpl22-HA expression under the *Eef1a* promoter in CAMK2α-positive excitatory neurons. **b**, Representative illustration of target area for bilateral AAV-DIO-RiboTag injection in the dorsal hippocampus. Tagged ribosomes from Rpl22-HA-expressing CAMK2α-positive excitatory neurons were recovered from total lysate by immunoprecipitation (IP) with magnetic beads conjugated to anti-HA antibodies. RNAs were extracted from the IP and total lysate. **c**, Immunohistochemistry for HA staining demonstrating that expression of AAV-DIO-RiboTag viral vector is restricted to the CAMK2α-positive excitatory neurons. Two independent experiments showed similar results. Scale bars: 200 μm. **d**–**g**, Comparison of RNA-Seq from IP to input showed an enrichment for excitatory neurons marker *Camk2a* and depletion of oligodendrocytes marker 2′, 3′-cyclic-nucleotide 3′ phosphodiesterase (CNPase, *Cnp*), astrocytes marker (*Gfap*) and markers of inhibitory neurons *Sst* and *Pvalb*, indicating a successful immunoprecipitation from excitatory neurons.

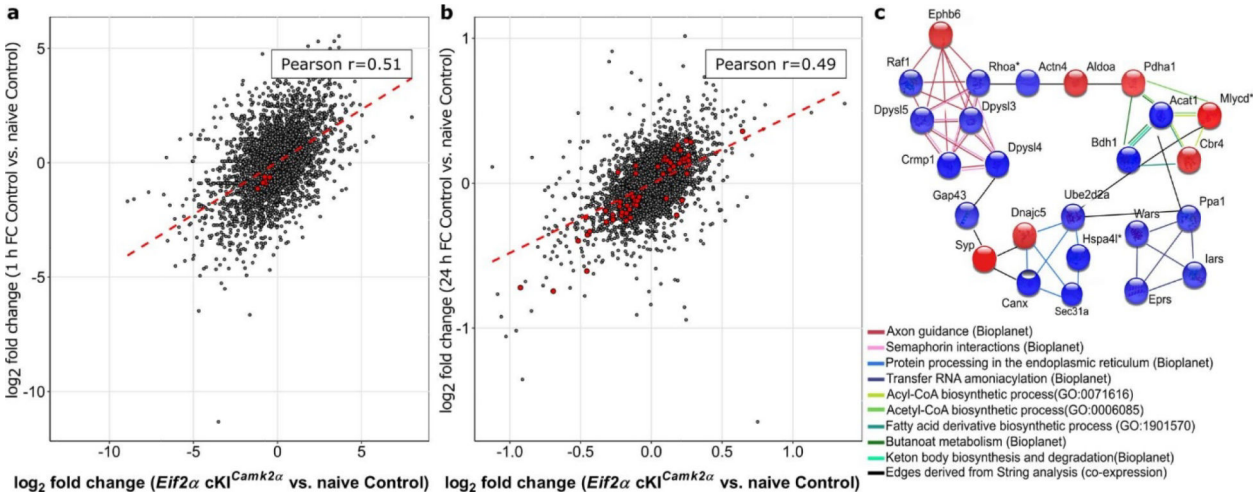

Extended Data Fig. 5. Analysis of excitatory neurons-specific translational landscape and proteomics from hippocampi of *Eif2a* cKI^{Camk2a} mice and following fear conditioning learning.

a, Pairwise Pearson correlation coefficient between log2 fold changes in translation efficiency comparing the genotype effect (naive *Eif2a* cKI^{Camk2a} vs. naive control) and learning effect (1 h fear conditioning control vs. naive control) using all translated mRNAs (11,805 transcripts). **b**, Pairwise Pearson correlation coefficient between log2 fold changes in protein levels comparing the genotype effect (naive *Eif2a* cKI^{Camk2a} vs. naive control) and learning effect (24 h fear conditioning control vs. naive control) using all CA1 expressed proteins (5,237 proteins). Pearson correlation coefficients were significant in both cases ($P <$ 0.0001), dots marked red denote transcripts/proteins differentially translated/expressed. **c**, Functional enrichment in protein subset similarity differentially expressed between proteomes of the two genotypes (52 proteins), and between proteomes of treatment vs. naive mice from both genotypes (27 proteins). GO ontologies, BioPlanet pathways and Reactome pathways showing significant enrichment (FDR adjusted $P < 0.1$) are presented. Nodes represent proteins, edges represent pathway/ontology relatedness. Black edges are links found by String analysis and represent co-expression evidence. Blue nodes denote reduced level of expression; red nodes denote increased level of expression. * denote proteins differentially expressed following 24 h fear conditioning in both mouse genotypes, but not between naive mice.

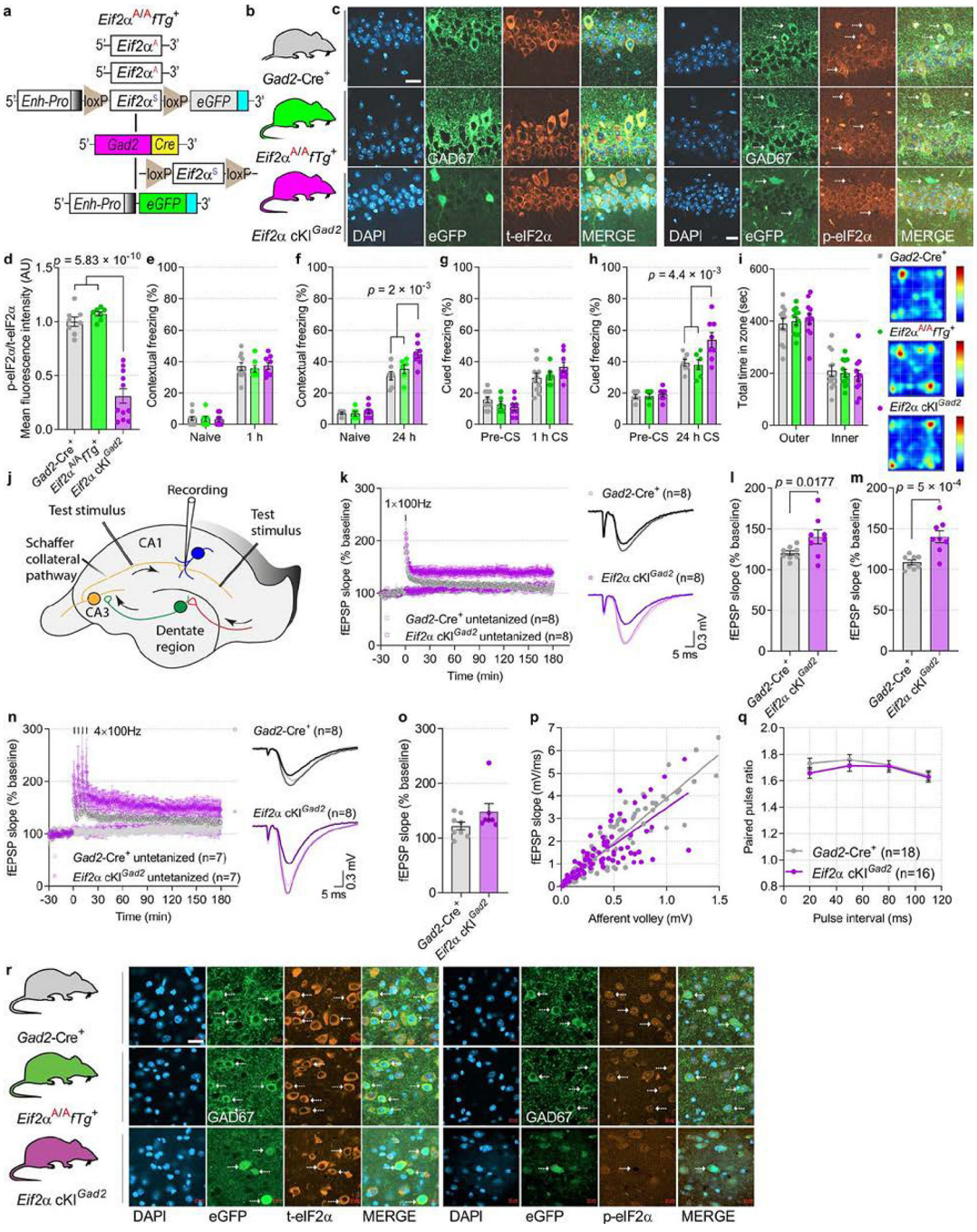

Extended Data Fig. 6. Consolidation of contextual and auditory fear memory and L-LTP induction is facilitated in *Eif2a* cKI^{Gad2} mice.

a, **b**, Schematic of the breeding strategy to generate *Eif2a* cKI^{Gad2} mice by crossing *Eif2a*$^{A/A}$*fTg*$^{+}$ mice with a *Gad2*-Cre^{+} transgenic line and the three genotypes of mice used in experiments. **c**, Immunofluorescent labelling of GAD67-positive neurons shows a decrease in p-eIF2α but no change in t-eIF2α in the CA1 region of *Eif2a* cKI^{Gad2} compared to control mice. Two independent experiments showed similar results. eGFP expression indicates the successful Cre recombinase-mediated deletion of WT *Eif2a fTg* in GAD2^{+}

GABAergic inhibitory neurons. **d**, Quantitative analyses of p-eIF2α levels in control and *Eif2a* cKI^{Gad2} mice ($F_{2, 23}$ = 61.6; n = 8, 7, 11, points represent means per mouse). In *Eif2a* cKI^{Gad2} mice, deletion of the floxed transgene significantly reduced p-eIF2α levels. **e**, Short-term contextual fear memory is not enhanced in *Eif2a* cKI^{Gad2} mice ($F_{2, 44}$ = 0.084; n = 10, 7, 8). **f**, Long-term contextual fear memory is enhanced in *Eif2a* cKI^{Gad2} mice ($F_{2, 36}$ = 7.41; n = 7, 6, 8). **g**, Short-term auditory fear memory is not altered in *Eif2a* cKI^{Gad2} mice ($F_{2, 42}$ = 0.24; n = 10, 6, 8). **h**, Long-term auditory fear memory is enhanced in *Eif2a* cKI^{Gad2} mice ($F_{2, 36}$ = 6.32; n = 7, 6, 8). **i**, In an open field test, all groups spent a similar amount of time in the outer versus inner zones ($F_{2, 64}$ = 9.8 × 10^{-12}; n = 12, 12, 11). Representative group-average heat-map of travelled path in an open field arena. **j**, Experimental scheme in acute hippocampal slices: Schaffer collateral fibres were stimulated in two independent pathways with extracellular electrodes and fEPSPs were recorded in CA1 stratum radiatum. **k**–**m**, A single high-frequency train elicited E-LTP and generated a sustained L-LTP in *Eif2a* cKI^{Gad2} slices ($F_{1, 7}$ = 6.9; n = 8, 8). **n**–**o**, L-LTP induced by four high frequency trains is similar in *Gad2*-Cre^{+} and *Eif2a* cKI^{Gad2} slices (**o**, L-LTP, $F_{1, 7}$ = 3.03; n = 8, 7). **p**, fEPSP versus fibre volley were fitted similarly by linear regression (R^2 = 0.84 for *Gad2*-Cre^{+} and R^2 = 0.58 for *Eif2a* cKI^{Gad2} slices). **q**, PPF did not differ between *Gad2*-Cre^{+} and *Eif2a* cKI^{Gad2} slices (two-way ANOVA, $F_{1, 128}$ = 1.54; n_{mice} = 18, 16, points represent group means). **r**, Immunofluorescent labelling of inhibitory interneurons in amygdala showing a decrease in p-eIF2α levels. Two independent experiments showed similar results. Data are presented as mean ± s.e.m. in **d**–**i**, **k**–**q**. p-values by one-way ANOVA followed by Tukey's multiple comparisons post hoc test in **d**; two-way ANOVA in **f** and **h** followed by Tukey's multiple comparisons post hoc test; two-way ANOVA (repeated measurements) in **l** and **m** followed by Sidak's multiple comparisons post hoc test are indicated. Points represent individual mice unless stated otherwise. Scale bars: 20 μm. Calibration: 0.3 mV, 5 ms.

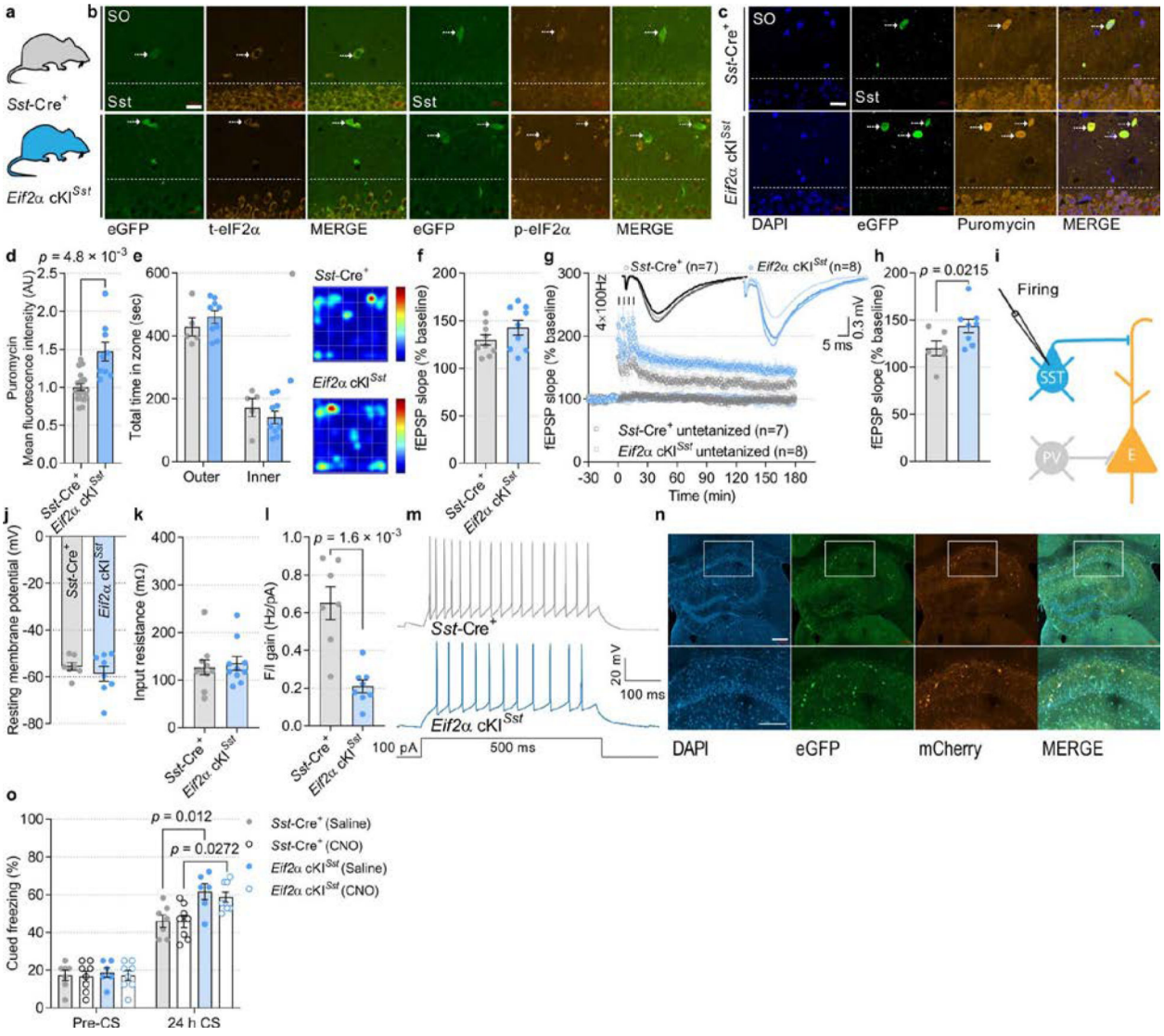

Extended Data Fig. 7. Somatostatin-specific reduction of p-eIF2α facilitates L-LTP.

a, **b**, Immunofluorescent labelling of total and p-eIF2α in SST^{+} neurons in the CA1 region shows reduced p-eIF2α levels in cKI mice. Two independent experiments showed similar results. **c**, **d**, iSUnSET shows enhanced protein synthesis in *Eif2a* cKI^{Sst} mice ($t_{10.11} = 3.6$; $n = 18, 9$, points represent means per mouse). Two independent experiments showed similar results. **e**, Both groups spent a similar amount of time in the outer and inner zones during an open field test ($F_{1, 24} = 7.1 \times 10^{-10}$; $n = 5, 9$). Representative group-average heat-map of travelled path in the test arena. **f**, A single high-frequency train (1 × HFS for 1 s) induces similar E-LTP (30 min post-HFS) in *Sst*-Cre^{+} and *Eif2a* cKI^{Sst} slices. **g**, **h**, Four tetanic trains at 100 Hz induce a facilitated L-LTP in *Eif2a* cKI^{Sst} slices (**h**, L-LTP, $F_{1, 7} = 9.531$; $n = 6, 8$). **i**, Diagram of experimental arrangement for recording intrinsic and firing properties in somatostatin neuron. **j**, Resting membrane potential ($t_{10.43} = 0.86$; $n = 7, 8$). **k**, Input resistance ($t_{17.92} = 0.38$; $n = 10, 10$). **l**, The frequency-current (F/I gain) relationship is reduced in *Eif2a* cKI^{Sst} mice ($t_{7.825} = 4.7$; $n = 7, 8$). **m**, Example of traces obtained in response to 100 pA current injection in somatostatin-expressing interneurons in *Sst*-Cre^{+} and

Eif2a cKI^{Sst} mice. **n**, Representative illustration of target area for the injection of AAV9-EF1α-DIO-EYFP-WPRE-hGH to label SST-expressing neurons in the dorsal hippocampus. Two independent experiments showed similar results. **o**, Overview image from an *Eif2a* cKI^{Sst} mouse in which the CA1 was injected with the Cre-dependent AAV9-DIO-hM4D(Gi)-mCherry (hM4Di) virus. Two independent experiments showed similar results. **p**, No effect on cued freezing by silencing CA1 SST^{+} neurons following fear conditioning in control and *Eif2a* cKI^{Sst} mice ($F_{3, 50} = 4.38$; $n = 7, 8, 6, 8$). Data are presented as mean ± s.e.m. in **d**–**h**, **j**–**l**, **p**. *p*-values by two-tailed unpaired *t*-test with Welch's correction in **d** and **l;** and by mixed-effects model REML in **h** followed by Sidak's multiple comparisons post hoc test are indicated; two-way ANOVA in **p** followed by Sidak's multiple comparisons post hoc test. Points represent individual mice unless stated otherwise. Scale bars: 200 μm. Calibration: 0.3 mV, 5 ms.

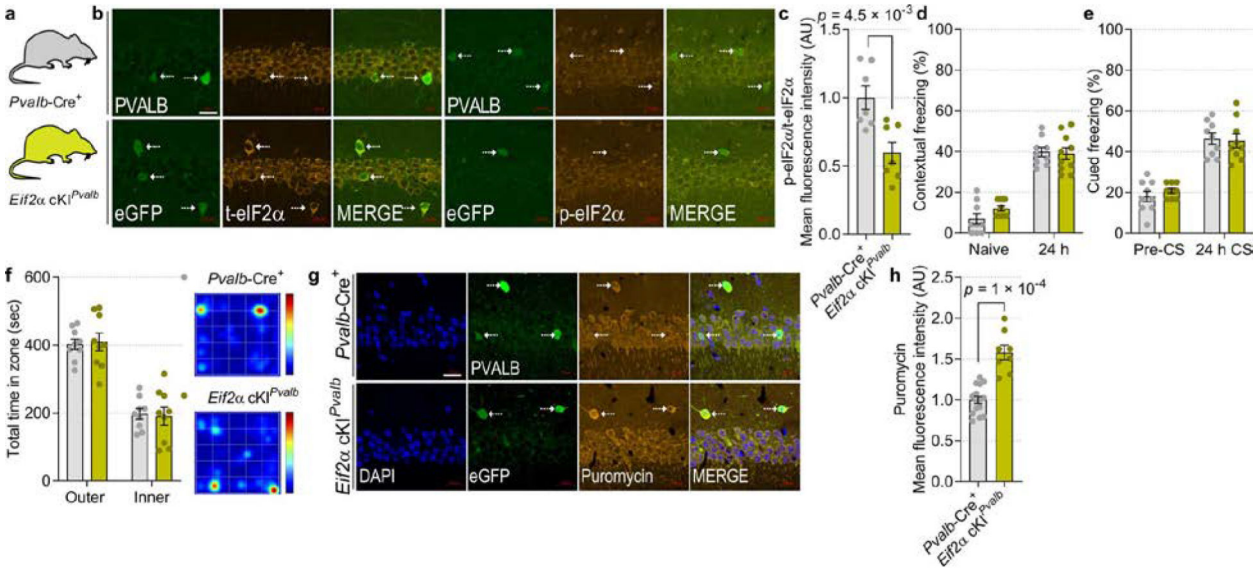

Extended Data Fig. 8. *Eif2a* cKI^{Pvalb} mice show no change in consolidation of contextual and auditory fear memory.

a, Diagram depicts the genotypes of mice used in the experiments. **b**, **c**, Immunofluorescent labelling of total and p-eIF2α in PVALB^{+} neurons shows reduced p-eIF2α levels in *Eif2a* cKI^{Pvalb} mice ($t_{11.86} = 3.5$; $n = 7, 7$, points represent means per mouse). Two independent experiments showed similar results. **d**, Long-term contextual fear memory is not changed in *Eif2a* cKI^{Pvalb} mice ($F_{1, 34} = 0.85$; $n = 9, 10$). **e**, Long-term auditory fear memory remains intact in *Eif2a* cKI^{Pvalb} mice ($F_{1, 32} = 0.124$; $n = 9, 9$). **f**, In an open field test, both groups spent a similar amount of time in the outer and inner zones ($F_{1, 32} = 6.6 \times 10^{-12}$; $n = 9, 9$). Representative heat-map of travelled path in an open field arena. **g**, **h**, Immunohistochemistry of puromycin in *Eif2a* cKI^{Pvalb} shows enhanced protein synthesis ($t_{10.67} = 5.85$; $n = 15, 8$, points represent means per mouse). Two independent experiments showed similar results. Data are presented as mean ± s.e.m. in **c**–**f**, **h**. *p*-values by two-tailed unpaired *t*-test with Welch's correction in **c** and **h** are indicated. Points represent individual mice unless stated otherwise. Scale bars: 20 μm.

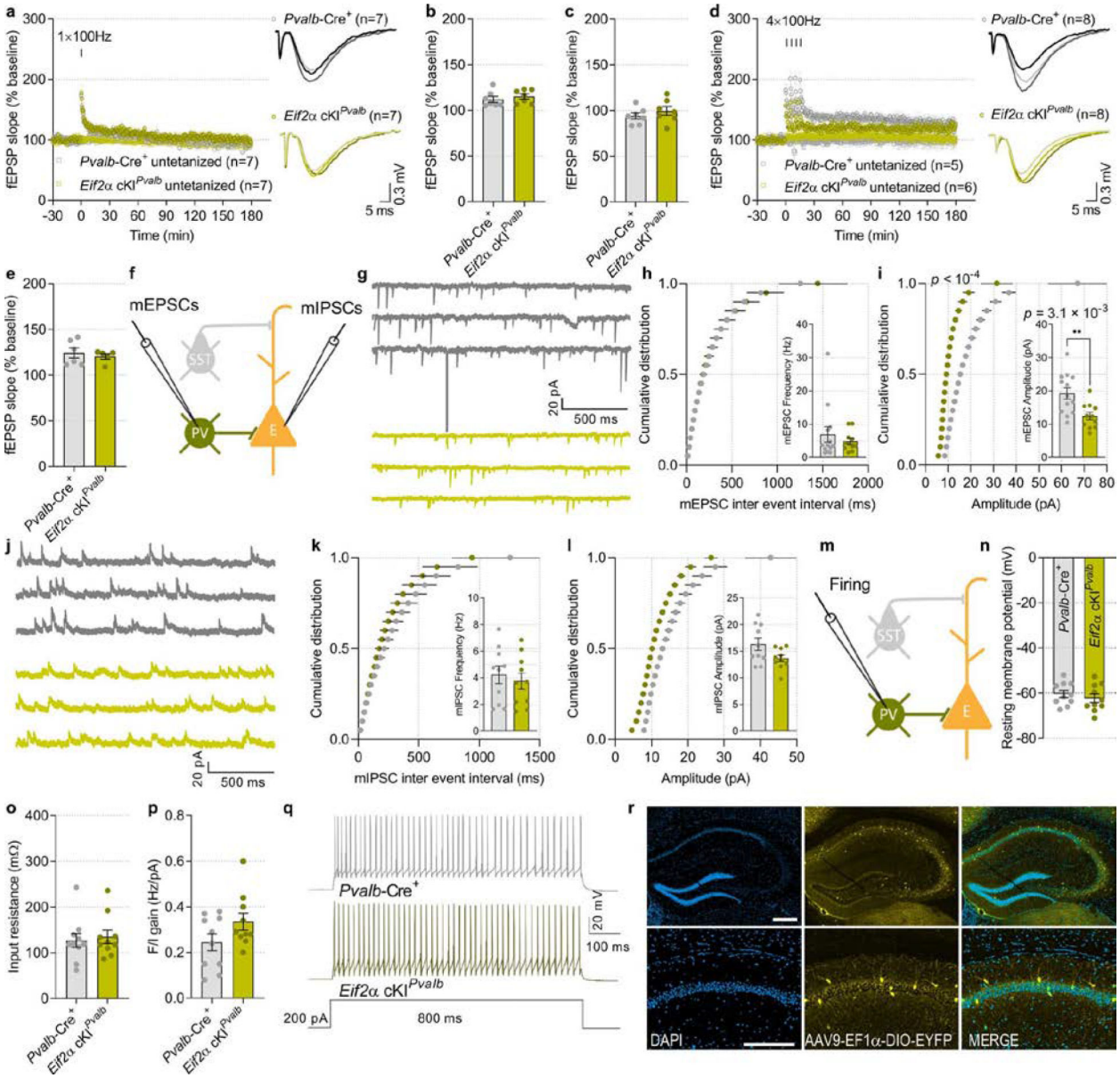

Extended Data Fig. 9. No change in L-LTP threshold in *Eif2a* cKI^{Pvalb} mice.

a–**c**, A 1 × HFS induced short-lasting E-LTP in *Pvalb*-Cre^{+} and *Eif2a* cKI^{Pvalb} hippocampal slices (E-LTP, $F_{1,\,6} = 1.917$; $n = 7, 7$). **d**, **e**, L-LTP induced by four tetanic trains at 100 Hz is similar in *Pvalb*-Cre^{+} and *Eif2a* cKI^{Pvalb} slices (**e**; L-LTP, $t_{7.542} = 0.6136$; $n = 6, 5$). **f**, Diagram of experimental arrangement with whole cell recording of mEPSCs (in PVALB^{+}) and mIPSCs (in excitatory neurons). **g**, Sample traces of mEPSCs. **h**, Cumulative distribution of mEPSC inter-event intervals ($n_{mice} = 13, 11$, points represent group means). Inset shows similar mEPSC frequency in *Pvalb*-Cre^{+} and *Eif2a* cKI^{Pvalb} ($t_{15.41} = 0.84$; $n = 13, 11$). **i**, Cumulative distribution of mEPSC amplitudes ($n_{mice} = 13, 11$, points represent group means). Bar graph in inset shows reduced mEPSC amplitude in *Eif2a* cKI^{Pvalb} ($t_{20.34} = 3.35$; $n = 13, 11$). **j**, Sample traces of mIPSCs. **k**, Cumulative distribution of mIPSC inter-event intervals ($n_{mice} = 10, 10$, points represent group means). Inset shows similar mIPSC

frequency ($t_{17.83} = 0.52$; $n = 10, 10$). **l**, Cumulative distribution of mIPSC amplitudes ($n_{mice} = 10, 10$, points represent group means). Inset, mIPSC amplitude is not changed between the groups ($t_{13.70} = 2.04$; $n = 10, 10$). **m**, Diagram of experimental arrangement for recording intrinsic and firing properties from parvalbumin neuron. **n**, Resting membrane potential ($t_{17.55} = 0.79$; $n = 10, 10$). **o**, Input resistance ($t_{17.92} = 0.38$; $n = 10, 10$). **p**, The F/I gain relationship is similar in the *Pvalb*-Cre^{+} and *Eif2a* cKI^{Pvalb} mice ($t_{18} = 1.72$; $n = 10, 10$). **q**, Representative traces obtained in response to 200 pA current injection in the parvalbumin-expressing interneurons from *Pvalb*-Cre^{+} and *Eif2a* cKI^{Pvalb} mice. **r**, Representative illustration of target area for the injection of AAV9-EF1α-DIO-EYFP-WPRE-hGH to label PVALB-expressing neurons in the dorsal hippocampus. Two independent experiments showed similar results. Data are presented as mean ± s.e.m. in **a**–**e**, **h**, **i**, **k**, **l**, **n**–**p**. *p*-values by Kolmogorov–Smirnov test in **i** and by two-tailed unpaired *t*-test with Welch's correction in **i**(inset) are indicated. Points represent individual mice unless stated otherwise. Scale bars: 200 μm. Calibration: 0.3 mV, 5 ms.

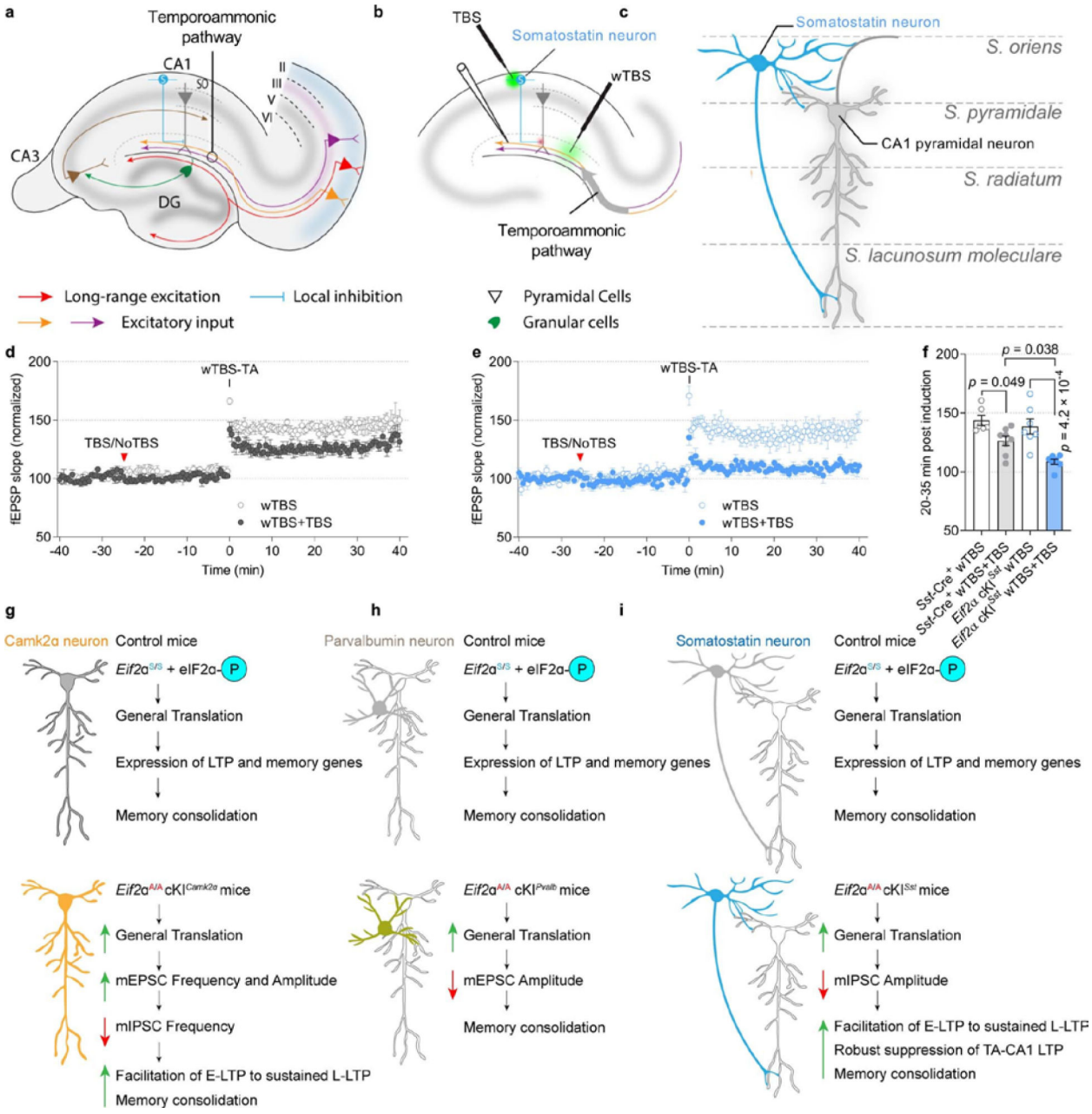

Extended Data Fig. 10. TBS-induced LTP in CA1 oriens/alveus (O/A) somatostatin-expressing interneurons exerts a more robust suppression of TA-CA1 LTP in *Eif2a* cKI^{Sst} mice.

a–**c**, Schematic of experimental setup in acute hippocampal slices: Temporoammonic afferents from the entorhinal cortex were stimulated by a weak TBS (wTBS) in presence or absence of prior TBS in CA1 oriens/alveus (O/A) region and fEPSPs were recorded in stratum lacunosum-moleculare of CA1. **d**, In *Sst*-Cre^{+} hippocampal slices, TBS in CA1-O/A region suppresses LTP of TA-CA1 field excitatory postsynaptic potentials (fEPSPs) when compared to slices with No-TBS in CA1-O/A region. **e**, In *Eif2a* cKI^{Sst} hippocampal slices, TBS in CA1-O/A region also reduces TA-LTP relative to slices with No-TBS in CA1-O/A region. **f**, Summary plots of normalized LTP magnitude in TA-CA1 pathway. TBS at CA1-

O/A supress TA-CA1 pathway in *Sst*-Cre^{+} ($F_{3, 24}$ = 11.85; n = 6, 8, points represent individual mice) and *Eif2a* cKI^{Sst} ($F_{3, 24}$ = 11.85; n = 7, 7, points represent individual mice). However, the magnitude of suppression is larger in *Eif2a* cKI^{Sst} than in *Sst*-Cre^{+} mice ($F_{3, 24}$ = 11.85; n = 8, 7, points represent individual mice). **g**, Reduction of p-eIF2α in CAMK2α-expressing excitatory neurons facilitates L-LTP and excitatory synaptic transmission (amplitude and frequency of mEPSCs), reduces inhibitory synaptic transmission (frequency of mIPSCs) and enhances memory consolidation (fear conditioning). **h**, Ablation of p-eIF2α in parvalbumin-expressing neurons causes a reduction in mEPSC amplitude without affecting threshold for L-LTP induction or consolidation of fear memory. **i**, Depletion of p-eIF2α in somatostatin-expressing neurons facilitates L-LTP and consolidation of fear memory by reducing the amplitude of mIPSCs in pyramidal neurons and enhancing suppression of LTP in the TA pathway. Data are presented as mean ± s.e.m. in **d**–**f**. *p*-values by one-way ANOVA followed by Tukey's multiple comparisons post hoc test in **f** are indicated.

Supplementary Material

Refer to Web version on PubMed Central for supplementary material.

Acknowledgements

This study was supported by a Canada's International Development Research Centre (IDRC), in partnership with the Azrieli Foundation, the Canadian Institutes of Health Research (CIHR), and the Israel Science Foundation (ISF) to K.R. and N.S. J.-C.L. is supported by a CIHR Project grant (PJT-153311) and a Canada Research Chair in Cellular and Molecular Neurophysiology (CRC-950-231066). R.J.K. is supported by National Institutes of Health (NIH) Project grants (R01 DK113171, R01 DK103185, R01 CA198103 and R01 AG062190). E.S. is supported by the Ministerio de Ciencia, Innovación y Universidades (RTI2018-101838-J-I00) and A.Q. is supported by the European Research Council (ERC-2014-StG-638106), Ministerio de Economíay Competitividad (SAF2017-88108-R) and Agència de Gestió d'Ajuts Universitaris i de Recerca (2017SGR- 323). M.C.-M. is supported by the National Institute of Neurological Disorders and Stroke grant (2R01 NS076708-06 NINDS). Support to R.S. was provided by Richard and Edith Strauss Postdoctoral Fellowships in Medicine. We thank the CNAG-CRG for assistance with RNA sequencing; G. S. McKnight for the RPL22-HA plasmid; members of the Sonenberg laboratory, specifically I. Harvey, A. Lafrance, A. Sylvestre, E. Migon and S. Murthy, as well as I. Laplante, H. Hall, M. Anadolu and K. Gamache for support with animals and resources; and S. Tahmasebi for critical reading of the manuscript.

References

1. Santini E, Huynh TN & Klann E Mechanisms of translation control underlying long-lasting synaptic plasticity and the consolidation of long-term memory. Prog. Mol. Biol. Transl. Sci 122, 131–167 (2014). [PubMed: 24484700]
2. Gal-Ben-Ari S et al. Consolidation and translation regulation. Learn. Mem 19, 410–422 (2012). [PubMed: 22904372]
3. Costa-Mattioli M, Sossin WS, Klann E & Sonenberg N Translational control of long-lasting synaptic plasticity and memory. Neuron 61, 10–26 (2009). [PubMed: 19146809]
4. Costa-Mattioli M & Walter P The integrated stress response: from mechanism to disease. Science 368, eaat5314 (2020). [PubMed: 32327570]
5. Sonenberg N, Morgan MA, Merrick WC & Shatkin AJ A polypeptide in eukaryotic initiation factors that crosslinks specifically to the 5'-terminal cap in mRNA. Proc. Natl Acad. Sci. USA 75, 4843–4847 (1978). [PubMed: 217002]
6. Kahvejian A, Svitkin YV, Sukarieh R, M'Boutchou MN & Sonenberg N Mammalian poly(A)-binding protein is a eukaryotic translation initiation factor, which acts via multiple mechanisms. Genes Dev. 19, 104–113 (2005). [PubMed: 15630022]

7. Sonenberg N & Dever TE Eukaryotic translation initiation factors and regulators. Curr. Opin. Struct. Biol 13, 56–63 (2003). [PubMed: 12581660]
8. Klann E & Sweatt JD Altered protein synthesis is a trigger for long-term memory formation. Neurobiol. Learn. Mem 89, 247–259 (2008). [PubMed: 17919940]
9. Kandel ER The molecular biology of memory storage: a dialogue between genes and synapses. Science 294, 1030–1038 (2001). [PubMed: 11691980]
10. McGaugh JL et al. Memory—a century of consolidation. Science 287, 248–251 (2000). [PubMed: 10634773]
11. Costa-Mattioli M et al. eIF2α phosphorylation bidirectionally regulates the switch from short- to long-term synaptic plasticity and memory. Cell 129, 195–206 (2007). [PubMed: 17418795]
12. Costa-Mattioli M et al. Translational control of hippocampal synaptic plasticity and memory by the eIF2α kinase GCN2. Nature 436, 1166–1173 (2005). [PubMed: 16121183]
13. Batista G, Johnson JL, Dominguez E & Costa-Mattioli M Translational control of auditory imprinting and structural plasticity by eIF2α. eLife 5, e17197 (2016). [PubMed: 28009255]
14. Ounallah-Saad H, Sharma V, Edry E & Rosenblum K Genetic or pharmacological reduction of PERK enhances cortical-dependent taste learning. J. Neurosci 34, 14624–14632 (2014). [PubMed: 25355215]
15. Sharma V et al. Local inhibition of PERK enhances memory and reverses age-related deterioration of cognitive and neuronal properties. J. Neurosci 38, 648–658 (2018). [PubMed: 29196323]
16. Costa-Mattioli M et al. Translational control of hippocampal synaptic plasticity and memory by the eIF2α kinase GCN2. Nature 436, 1166–1173 (2005). [PubMed: 16121183]
17. Zhu PJ et al. Suppression of PKR promotes network excitability and enhanced cognition by interferon-γ-mediated disinhibition. Cell 147, 1384–1396 (2011). [PubMed: 22153080]
18. Ma T et al. Suppression of eIF2α kinases alleviates Alzheimer's disease-related plasticity and memory deficits. Nat. Neurosci 16, 1299–1305 (2013). [PubMed: 23933749]
19. Back SH et al. Translation attenuation through eIF2α phosphorylation prevents oxidative stress and maintains the differentiated state in β cells. Cell Metab. 10, 13–26 (2009). [PubMed: 19583950]
20. Kedersha N et al. Evidence that ternary complex (eIF2-GTP-tRNA(i)(Met))-deficient preinitiation complexes are core constituents of mammalian stress granules. Mol. Biol. Cell 13, 195–210 (2002). [PubMed: 11809833]
21. Bliss TV & Lomo T Long-lasting potentiation of synaptic transmission in the dentate area of the anaesthetized rabbit following stimulation of the perforant path. J. Physiol. (Lond.) 232, 331–356 (1973). [PubMed: 4727084]
22. Bliss TV & Collingridge GL A synaptic model of memory: long-term potentiation in the hippocampus. Nature 361, 31–39 (1993). [PubMed: 8421494]
23. Kelleher RJ III, Govindarajan A & Tonegawa S Translational regulatory mechanisms in persistent forms of synaptic plasticity. Neuron 44, 59–73 (2004). [PubMed: 15450160]
24. Takeuchi T, Duszkiewicz AJ & Morris RG The synaptic plasticity and memory hypothesis: encoding, storage and persistence. Phil. Trans. R. Soc. Lond. B 369, 20130288 (2013). [PubMed: 24298167]
25. Xu H et al. A disinhibitory microcircuit mediates conditioned social fear in the prefrontal cortex. Neuron 102, 668–682.e5 (2019). [PubMed: 30898376]
26. Yu K, Garcia da Silva P, Albeanu DF & Li B Central amygdala somatostatin neurons gate passive and active defensive behaviors. J. Neurosci 36, 6488–6496 (2016). [PubMed: 27307236]
27. Lovett-Barron M et al. Dendritic inhibition in the hippocampus supports fear learning. Science 343, 857–863 (2014). [PubMed: 24558155]
28. Leão RN et al. OLM interneurons differentially modulate CA3 and entorhinal inputs to hippocampal CA1 neurons. Nat. Neurosci 15, 1524–1530 (2012). [PubMed: 23042082]
29. Sonenberg N & Hinnebusch AG Regulation of translation initiation in eukaryotes: mechanisms and biological targets. Cell 136, 731–745 (2009). [PubMed: 19239892]
30. Zhang SY, Xu M, Miao QL, Poo MM & Zhang XH Endocannabinoid-dependent homeostatic regulation of inhibitory synapses by miniature excitatory synaptic activities. J. Neurosci 29, 13222–13231 (2009). [PubMed: 19846710]

31. Li H et al. Experience-dependent modification of a central amygdala fear circuit. Nat. Neurosci 16, 332–339 (2013). [PubMed: 23354330]
32. Chen SX, Kim AN, Peters AJ & Komiyama T Subtype-specific plasticity of inhibitory circuits in motor cortex during motor learning. Nat. Neurosci 18, 1109–1115 (2015). [PubMed: 26098758]
33. Fraklin KBJ & Paxinos G The Mouse Brain in Stereotaxic Coordinates 3rd edn (Academic, 2007).
34. Artinian J et al. Regulation of hippocampal memory by mTORC1 in somatostatin interneurons. J. Neurosci 39, 8439–8456 (2019). [PubMed: 31519824]
35. Tricoire L et al. A blueprint for the spatiotemporal origins of mouse hippocampal interneuron diversity. J. Neurosci 31, 10948–10970 (2011). [PubMed: 21795545]
36. Possemato AP et al. Multiplexed phosphoproteomic profiling using titanium dioxide and immunoaffinity enrichments reveals complementary phosphorylation events. J. Proteome Res 16, 1506–1514 (2017). [PubMed: 28171727]
37. Stokes MP et al. Complementary PTM profiling of drug response in human gastric carcinoma by immunoaffinity and IMAC methods with total proteome analysis. Proteomes 3, 160–183 (2015). [PubMed: 28248267]
38. Eng JK, McCormack AL & Yates JR An approach to correlate tandem mass spectral data of peptides with amino acid sequences in a protein database. J. Am. Soc. Mass Spectrom 5, 976–989 (1994). [PubMed: 24226387]
39. Villén J, Beausoleil SA, Gerber SA & Gygi SP Large-scale phosphorylation analysis of mouse liver. Proc. Natl Acad. Sci. USA 104, 1488–1493 (2007). [PubMed: 17242355]
40. Huttlin EL et al. A tissue-specific atlas of mouse protein phosphorylation and expression. Cell 143, 1174–1189 (2010). [PubMed: 21183079]
41. Sanz E, Bean JC, Carey DP, Quintana A & McKnight GS RiboTag: ribosomal tagging strategy to analyze cell-type-specific mRNA expression in vivo. Curr. Protoc. Neurosci 88, e77 (2019). [PubMed: 31216392]
42. Sanz E et al. Cell-type-specific isolation of ribosome-associated mRNA from complex tissues. Proc. Natl Acad. Sci. USA 106, 13939–13944 (2009). [PubMed: 19666516]
43. Langmead B, Trapnell C, Pop M & Salzberg SL Ultrafast and memory-efficient alignment of short DNA sequences to the human genome. Genome Biol 10, R25 (2009). [PubMed: 19261174]
44. Frankish A et al. GENCODE reference annotation for the human and mouse genomes. Nucleic Acids Res. 47, D766–D773 (2019). [PubMed: 30357393]
45. Love MI, Huber W & Anders S Moderated estimation of fold change and dispersion for RNA-seq data with DESeq2. Genome Biol. 15, 550 (2014). [PubMed: 25516281]
46. Kuleshov MV et al. Enrichr: a comprehensive gene set enrichment analysis web server 2016 update. Nucleic Acids Res. 44, W90–W97 (2016). [PubMed: 27141961]

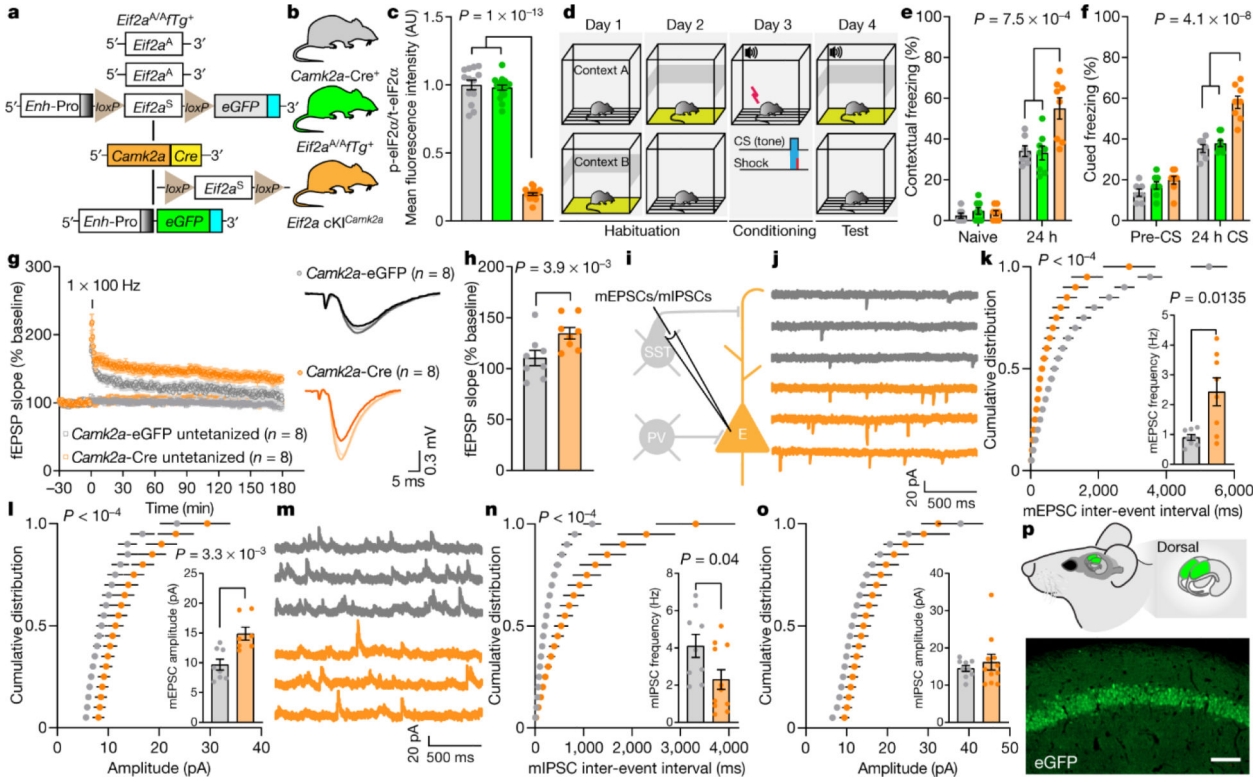

Fig. 1: Reduction of p-eIF2α in excitatory neurons facilitates memory consolidation, LTP and excitatory synaptic transmission, and reduces inhibitory synaptic transmission.

a, The genetic components of the *Eif2a*$^{A/A}$*fTg*$^{+}$ mice. eGFP expression in the *Eif2a* cKI*Camk2a* mice indicates successful Cre recombinase-mediated deletion of the wild-type *Eif2a* floxed transgene in excitatory neurons. **b**, The three genotypes of mice used in these experiments. **c**, Quantitative analyses of immunofluorescence images showing p-eIF2α as a proportion of total (t-)eIF2α in control and *Eif2a* cKI*Camk2a* mice ($F_{2,45}$ = 493.75, n = 13, 17, 18, points represent means per mouse). In *Eif2a* cKI*Camk2a* mice, p-eIF2α levels are reduced owing to the deletion of the floxed transgene. **d**, Schematic of weak contextual and auditory fear conditioning. **e**, Long-term contextual memory is enhanced in *Eif2a* cKI*Camk2a* mice ($F_{2,40}$ = 8.66, n = 7, 8, 8). **f**, Long-term auditory fear memory is enhanced in *Eif2a* cKI*Camk2a* mice ($F_{2,40}$ = 26.81, n = 7, 8, 8). **g**, **h**, A single high-frequency train (1 × HFS for 1 s) generated sustained L-LTP in slices from mice injected with *Camk2a*–Cre (**h**, L-LTP 180 min post-HFS, $F_{1,7}$ = 8.2, n = 8, 8). **i**, Whole-cell recording for mEPSCs and mIPSCs and firing. PV, PVALB^{+} neuron. **j**, Representative traces of mEPSCs from CAMK2α–eGFP^{+} and CAMK2α–Cre^{+} neurons. **k**, Cumulative distribution of mEPSC inter-event intervals recorded from CA1 excitatory neurons in mice injected with *Camk2a*–eGFP or *Camk2a*–Cre (n_{mice} = 8, 8, points represent group means). Inset, increased mean frequency of mEPSCs in mice injected with *Camk2a*–Cre ($t_{7.59}$ = 3.2, n = 8, 8). **l**, Cumulative distribution plots showing mEPSC amplitude (n_{mice} = 8, 7, points represent group means). Inset, mEPSC amplitude is increased in *Camk2a*–Cre-injected mice ($t_{12.19}$ = 3.64, n = 8, 7). **m**, Representative mIPSC traces. **n**, Cumulative distribution of mIPSC inter-event intervals recorded from CA1 excitatory neurons in mice injected with *Camk2a*–eGFP or *Camk2a*–Cre (n_{mice} = 9, 11, points represent group means). Inset, mIPSC frequency was reduced in mice

injected with *Camk2a*–Cre ($t_{16.71}$ = 2.22, n = 9, 11). **o**, Cumulative distribution of mIPSC amplitudes (n_{mice} = 9, 11, points represent group means). Inset, average mIPSC amplitude ($t_{12.69}$ = 0.75, n = 9, 11). **p**, Target area for injection of *Camk2a*–eGFP and *Camk2a*–Cre and representative image of GFP-labelled CAMK2α$^+$ excitatory neurons in CA1 of dorsal hippocampus; representative of five independent experiments. Mean ± s.e.m. (**c**, **e**–**h**, **k**, **l**, **n**, **o**). One-way ANOVA (**c**), two-way ANOVA (**e**, **f**) followed by Tukey's multiple comparisons post-hoc test; two-way ANOVA (repeated measures) (**g**, **h**) with Sidak's multiple comparisons post-hoc test; Kolmogorov–Smirnov test (**k**, **l**, **n**); two-tailed unpaired *t*-test with Welch's correction (insets in **k**, **l**, **n**). Points represent individual mice unless stated otherwise. Scale bar, 100 μm.

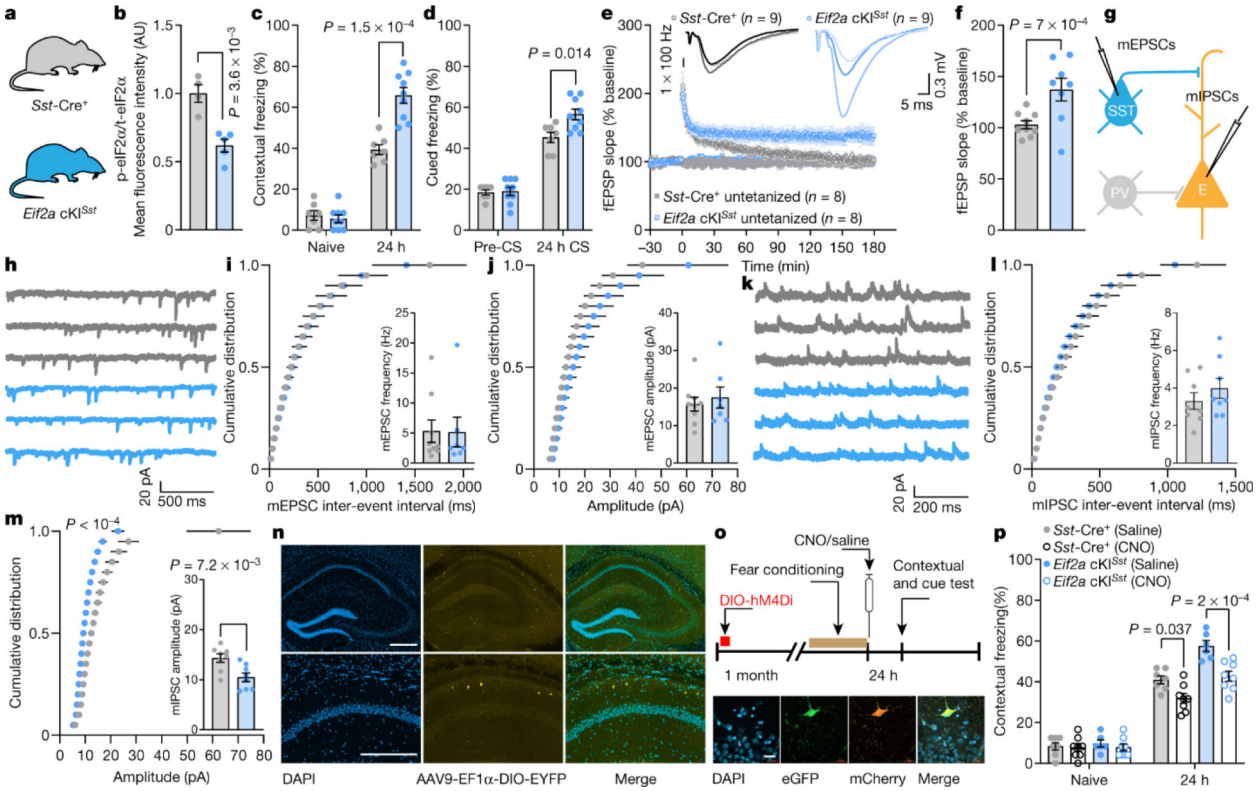

Fig. 2: Reduction in p-eIF2α in SST$^+$ neurons facilitates memory consolidation and LTP, and reduces inhibitory synaptic transmission onto CA1 pyramidal neurons.

a, The two genotypes of mice used. **b**, Quantification of total and p-eIF2α in CA1 SST$^+$ neurons shows reduced p-eIF2α in *Eif2a* cKI^{Sst} mice ($t_{5.79}$ = 4.73, n = 4, 5, points represent means per mouse). **c**, **d**, Long-term contextual memory (**c**; $F_{1, 28}$ = 19.19, n = 7, 9) and long-term auditory fear memory (**d**; $F_{1, 28}$ = 6.86, n = 7, 9) are enhanced in *Eif2a* cKI^{Sst} mice. **e**, **f**, A single high-frequency train (1 × HFS for 1 s) leads to sustained LTP in *Eif2a* cKI^{Sst} slices 180 min later (**f**; L-LTP, $F_{1, 8}$ = 8.134, n = 9, 8). **g**, Experimental arrangement for whole-cell recording of mEPSCs (from SST$^+$ neurons) and mIPSCs (from excitatory neurons). **h**, Representative traces of mEPSCs recorded from *Sst*-Cre$^+$ and *Eif2a* cKI^{Sst} mice. **i**, Cumulative distribution of mEPSC inter-event intervals (n_{mice} = 9, 7, points represent group means). Inset, mEPSC frequency ($t_{11.85}$ = 0.05, n = 9, 7). **j**, Cumulative distribution of mEPSC amplitudes (n_{mice} = 9, 7, points represent group means). Inset, average mEPSC amplitude ($t_{10.69}$ = 0.52, n = 9, 7). **k**, Sample traces of mIPSCs recorded from CA1 excitatory neurons in *Sst*-Cre$^+$ and *Eif2a* cKI^{Sst} mice. **l**, Cumulative distribution of mIPSC inter-event intervals (n_{mice} = 8, 8, points represent group means). Inset, mIPSC frequency ($t_{13.57}$ = 0.98, n = 8, 8). **m**, Cumulative distribution of mIPSC amplitudes (n_{mice} = 8, 8, points represent group means). Inset, mIPSC amplitude was reduced in *Eif2a* cKI^{Sst} mice (t_{14} = 3.14, n = 8, 8). **n**, Representative illustration of target area for the injection of AAV9-EF1α -DIO-EYFP-WPRE-hGH. Image shows labelled SST-expressing neurons in the dorsal hippocampus. Four independent experiments showed similar results. **o**, Top, timeline of DREADD experiments in fear conditioning paradigm immediately followed by injection of saline (control) or clozapine-*N*-oxide (CNO (silenced)). Bottom, images of brain

section from an *Eif2a* cKI^{Sst} mouse in which CA1 was injected with Cre-dependent AAV9-DIO-hM4D(Gi)-mCherry (hM4Di). Representative of two independent experiments. **p**, Chemogenetic inhibition of SST^{+} neurons in CA1 by CNO administration immediately after training attenuates consolidation of contextual fear memory in control and *Eif2a* cKI^{Sst} mice ($F_{3,50}$ = 13.7, n = 7, 8, 6, 8). Mean ± s.e.m. Two-tailed unpaired t-test with Welch's correction (**b**, insets in **i**, **j**, **l**, **m**); two-way ANOVA (**c**, **d**, **p**) followed by Sidak's multiple comparisons post-hoc test; mixed-effects model (restricted maximum likelihood (REML); **e**, **f**) followed by Sidak's multiple comparisons post-hoc test; Kolmogorov–Smirnov test (**m**). Points represent individual mice unless stated otherwise. Scale bars, 200 μm.